Downloaded from Plasma.com

INSTITUTE OF PHYSICS PUBLISHING JOURNAL OF PHYSICS D: APPLIED PHYSICS

J. Phys. D: Appl. Phys. **36** (2003) R53–R79 PII: S0022-3727(03)19407-7

TOPICAL REVIEW

Plasma display panels: physics, recent developments and key issues

J P Boeuf

CPAT, Université Paul Sabatier, 118 Route de Narbonne, 31062 Toulouse Cedex, France

E-mail: jpb@cpat.ups-tlse.fr

Received 29 August 2002
Published 26 February 2003
Online at stacks.iop.org/JPhysD/36/R53

Abstract
In this paper, we describe the principles of operation of a plasma display panel (PDP) and the physical mechanisms controlling the performances of a PDP in terms of light emission efficiency, lifetime and image quality. Emphasis is put on the physics of the plasma occurring in a PDP cell, on the discharge optimization, and on the analysis of recent results provided by experimental and numerical diagnostic tools. We focus on alternative current PDPs, where the plasma is generated by a dielectric barrier discharge, the configuration adopted by most PDP companies. The recent improvements and the remaining research issues are discussed.

1. Introduction

A plasma display panel (PDP) is essentially a matrix of sub-millimetre fluorescent lamps which are controlled in a complex way by electronic drivers. Each pixel of a PDP is composed of three elementary UV emitting discharge cells. The UV light is converted into visible light by phosphors in the three primary colours. The plasma in each cell of an alternative current (AC) PDP is generated by dielectric barrier discharges (DBDs) operating in a glow regime in a rare gas mixture (typically 500 Torr, 100 μm gap). The AC voltage is rectangular, with frequency of the order of 100 kHz, and rise time of about 200–300 ns. In the ON state, a current pulse of less than 100 ns duration flows through the cell at each half cycle.

PDPs have recently achieved good performance and their image quality can now compete with that of cathodic ray tubes (CRTs). PDPs up to 60 in. in diagonal have been demonstrated, some with high resolution. According to Standford Resources [1], more than 300 000 PDPs were sold worldwide in 2001 and the market should grow to 6 million units in 2007. The sales should switch from a business-dominated market (corporate board-room, public display applications) in 2001 to a television-dominated market in 2007. This prediction will become true only if the companies succeed in their efforts toward cost-reduction and if the PDP technology can keep up with competing technology such as liquid crystal displays (LCDs) and organic light emitting diodes (OLEDs). Although most of the LCD production is for diagonal sizes below 20 in., it now seems that LCDs will certainly overtake PDPs for TVs up to 30 in., and LCD manufacturers are actively working on larger sizes [2]. OLED is a younger but very promising technology and may become another competitor in the future. The success of PDPs will depend on cost-reduction in the different fabrication steps and on some technological improvements that must come out of the research labs in time [2].

In this paper we describe the basic mechanisms occurring in an AC PDP cell and the physics issues related to performance improvement. We also present the trends in the research toward better performance.

Section 2 contains a brief history of PDP research, and describes the characteristics of the recent PDPs and the needs for improvements. The principles of PDP operations (operating conditions, addressing methods) are described in section 3, with a brief sub-section on PDP manufacturing. Efficiency and lifetime issues (role of the gas mixture, operating conditions, materials) are discussed in section 4. Section 5 presents recent experimental and modelling diagnostics of the discharge plasma in a PDP cell. Recent research trends towards better performance (mainly related to efficiency) are summarized in section 6.

Downloaded from Plasma.com

2. Brief history and state of the art of PDPs

The use of discharge plasmas for information display started in the early 1950s, with the numeric indicator tube developed by Burroughs. This tube used the light from the negative glow around cathodes each shaped in the form of a numeral [3]. The PDP was invented in the 1960s at the Coordinated Science Laboratory at the University of Illinois where Bitzer and Slottow were developing displays for educational purpose. The idea was first to use a matrix of pixels at the intersections of line and column electrodes and to fire light emitting gas discharges at selected pixels. A glow discharge can be both an excellent switch and an efficient light source and this explains the persistence of researchers and companies during almost four decades to seek the goal of hang-on-the-wall colour television displays with diagonals up to 60 in. Developing the initial idea, Bitzer and Slottow realized the need for an insulating impedance at each discharge site. They considered the use of resistors, the eventual use of a resistive sheet, and finally the possibility of using a capacitive impedance instead of a resistive impedance. The use of resistors in series with each pixel led to the development of DC PDPs. The advantage of the capacitive impedance was that the capacitance could be part of the panel structure in a very simple way (dielectric layers above the electrodes) and should be easy to fabricate. Displays with capacitive impedance in series can obviously not be driven with DC voltages and this led to the concept of AC PDPs [4]. Bitzer and Slottow realized only later that the use of a capacitive coupling had other very important consequences and provided the inherent memory properties of AC PDPs. The history of this discovery is described in details by Slottow [5]. Other information on the early development of PDPs can be found in the review papers by Weber [6], Michel [7], and Sobel [8].

The initial PDPs were monochrome displays where Penning Ne–Ar mixtures (typically 0.1% Ar in Ne) were used and the light emitted by the discharges was due to the characteristic red–orange emission of neon. These displays were used for displaying complex technical information for various professional and military purposes. Research on colour PDPs started in the mid-1970s, and the first commercially available colour displays appeared in the late 1990s. In colour plasma displays, the gas mixture (Xe–Ne or Xe–Ne–He) emits UV photons which excite phosphors in the three fundamental colours. Each pixel is therefore associated with three micro-discharge cells. Various designs of plasma display have been proposed in the last 30 years. Three concepts were dominant till the end of the 1990s: the alternative current matrix (ACM) sustain structure, the alternative current coplanar (ACC) sustain structure, and the direct current with pulse-memory drive PDP. In the ACM structure the micro-discharges take place at the intersection of line and column electrodes covered by a dielectric layer, as in the original idea of Bitzer and Slottow. In the ACC structure (also called TSD, for three electrode surface discharge) developed in the early 1980s [9, 10], the sustain discharges occur between sets of parallel electrodes on the same plate, and addressing is provided by electrodes on the opposite plate, which are orthogonal to the coplanar electrodes. The initial design of this three-electrode structure was of a transmitting type, i.e. the discharge was behind the phosphor and the visible light was transmitted through the phosphor. A convincing (with respect to performance) ACC design was achieved only in a reflection type display that was developed in 1989 [10, 11]. In this structure, which is now the standard structure, the discharge is in front of the phosphor and the visible light is seen directly. The ACC structure has been recently adopted by most of the companies. Note that Dick and Biazzo [12, 13] had proposed in the 1970s the interesting concept of single substrate matrix or coplanar PDPs where all the electrodes are on the same glass plate. The DC PDP with pulse-memory drive [14, 15] has received considerable attention till the middle of the 1990s [16] and the feasibility of a 42 in. DC PDP was demonstrated. However, the performances (lifetime and efficacy) of DC PDPs were lower than those of AC PDPs, and this technology is now only marginally studied and developed. An important research effort had however been invested in DC PDPs and some of the concepts and ideas developed within this frame are worth remembering (see, e.g. the works on positive column discharges [17, 18] and Townsend discharges [19] for DC PDPs). The DC PDP will not be further discussed in this paper.

AC PDPs have now achieved a high level of performance. The first colour displays in the early 1990s had very low luminous efficacy (less than 1 lumen per Watt—lm W^{-1}) and low contrast. At the time this review is written, manufacturers report 1–2 lm W^{-1} efficacy for commercially available PDPs and 2–3 lm W^{-1} for laboratory samples [1]. The reported luminance is between 500 and 700 cd m^{-2} for 42–63 in. PDPs and the announced contrast ratios are 3000 : 1 in dark viewing conditions and 120 : 1 in bright light conditions. The reported lifetime can reach 30 000 h. The above numbers are cited by different manufacturers, and, since performance measurements are not yet standardized, it is difficult to know exactly what has been measured. From these numbers, however, it appears that an important research effort is still needed to improve the luminous efficacy which remains low compared to CRTs (about three times lower). An improvement of luminous efficacy will lead to cost reduction since it should lead to a decrease of the electronic drivers power requirements and thus of the driver cost, which is a large part of the total cost of a PDP. The trends in the research to achieve this goal is in the direction of more complex electrode shapes (within the ACC concept), optimization of cell geometry and gas mixture, material research (protective and emissive layer, phosphors) and optimization of addressing and sustaining schemes. In spite of the relatively large lifetime announced by the manufacturers, it seems that lifetime is still an issue. The initial brightness of a PDP is high (more than 500 cd m^{-2}), but the display quickly loses brightness over time [2]. This is due to the degradation of activated phosphors (the most vulnerable phosphor being the blue emitting one). The decrease of the luminance of a PDP can be as large as 10% in 5000 h [20] in normal operating conditions (the lifetime of the panel corresponds to a 50% decay of the luminance). The overall lifetime of a PDP also depends on the lifetime of the protective and emissive MgO layer and this parameter is not completely controlled. Another remaining issue concerning panel performance is related to image quality. Due to the way the grey scale is formed in a PDP, visible artefacts can form on the screen, especially when moving objects are displayed. These artefacts (called false contours) are corrected with

Downloaded from Plasma.com

sophisticated addressing schemes and dynamic false contour reducing methods [21]. Research is however still needed on this aspect.

Understanding the basic physics of the plasma dynamics, electron energy deposition and plasma–surface interactions is an essential part of the improvement of this technology. This is confirmed both by the dramatic increase in the number of papers published by research institutions on this topic in the last five years, and by the increasing number of high quality scientific papers recently published by company researchers in conference proceedings or in scientific journals.

3. DBDs for AC PDPs: principles and key parameters

Almost all the PDP companies have now adopted the AC PDP. In AC PDPs each cell consists of a microscopic DBD, i.e. the electrodes are covered with a dielectric layer 20–40 μm thick. Historically, DBDs have been applied to ozone production [22] in the mid 19th century, much before their use in displays. The application of DBD to the generation of VUV excimer radiation was proposed by Tanaka [23] in 1955. DBDs at atmospheric pressure can produce intense ultraviolet radiation that can be used to break molecular bonds and initiate photophysical and photochemical processes, and to modify surface properties. There are thus numerous potential applications of DBDs to material processing, thin-film deposition, pollution control, sterilization, and of course lighting (see Kogelschatz *et al* [22] and references therein). In the applications above, the DBDs generally operate at high pressure, for gap lengths of the order of 1 mm to a few cm. Under these large pd (pressure $\times$ gap length) conditions, the discharges operate in a streamer regime. Random transient filaments form in the electrode gap and are quenched due to the current limitation by the localized charge build-up on the dielectric layers. The applied voltage must change sign periodically in order to generate new discharges and new filaments. The voltage frequency is between 50 Hz and several hundred kHz in most applications. The limitation of the current due to the capacitive layers allows a good control of the power deposition in the volume, which would be impossible with metal electrodes in these atmospheric pressure and large gap length conditions.

In DBDs for PDPs, the electrode gap length is short, of the order of 100 μm, the pressure p is about 500 Torr and such that the pd product is of the order of a few Torr cm. For these small pd values, the discharges do not operate in a streamer regime but in a glow discharge regime. It is essential to operate in this regime because the ability to control each discharge separately and the reproducibility of the discharges are of paramount importance in a PDP. In this section we present the principles and operating conditions of a PDP. Emphasis is put on the physics but some of the more technological aspects (e.g. driving of a PDP panel, pixel size, high definition, etc) are also briefly discussed. The technological issues impose the constraints on the operating conditions of a PDP (e.g. addressing speed and response time of cell) and this is why a perfect understanding and control of the physics in a discharge cell is necessary.

3.1. Principles and operating conditions of AC PDPs

A plasma display consists of two glass plates separated by a gas gap of about 100 μm filled with a rare gas mixture (generally Xe–Ne or Xe–Ne–He) capable of emitting UV photons. Arrays of electrodes are deposited on each plate. The electrode arrays are covered by a 20–40 μm thick dielectric layer. The standard electrode geometry in the commercially available AC PDPs is the coplanar (ACC) electrode geometry. Although the ACC structure is by far the most developed electrode structure nowadays, we will also discuss the ACM electrode configuration in this section because the discharge properties and addressing schemes are very simple in that configuration. In the ACM configuration, arrays of parallel electrodes are deposited on each glass plate and the electrodes on the opposite faces are orthogonal to each other. A discharge can be initiated in the gas gap at the intersection of each line and column by applying appropriate voltages to the line and column electrodes (figure 1). Each discharge cell is therefore defined by two electrodes. In the ACC electrode configuration (figures 1 and 2) a discharge cell is defined by three electrodes: two parallel electrodes on one glass plate (front plate), and one electrode, orthogonal to the two coplanar electrodes, on the opposite glass plate (back plate).

The coplanar electrodes (also called display electrodes) in ACC PDPs are made of transparent conductive material (ITO). Their width is of the order of 200–300 μm in a 42 in. panel. Since the resistivity of ITO is not zero and the length of the electrodes can be as large as 1 m, a metal electrode of smaller width (bus electrode) is attached to each ITO

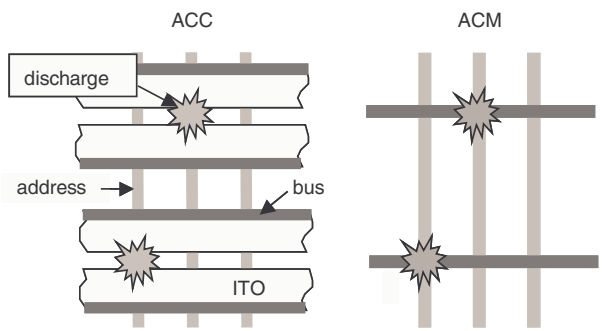

Figure 1. Coplanar (ACC) and matrix (ACM) electrode configurations of AC PDPs. The dielectric ribs are not represented (see figure 2).

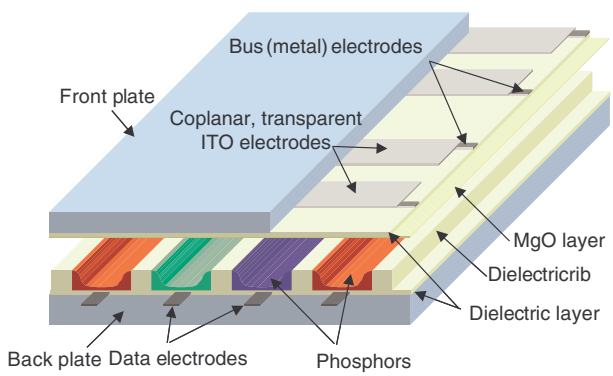

Figure 2. Simplified view of a coplanar PDP. The observer is on the front plate side.

Downloaded from Plasma.com

electrode to maintain a constant potential along the coplanar ITO electrodes. The data (or address) electrodes are metallic and their width is of the order of 80 μm in standard PDPs. Successive pairs of coplanar electrodes are separated by dielectric barrier 'rib' structures formed on the inner surfaces of the glass plates. A dielectric layer of thickness between 20 and 40 μm covers the address and coplanar electrodes. A MgO layer (about 500 nm) is deposited on the dielectric surface above the coplanar electrodes to protect the dielectric from sputtering and to provide large secondary electron emission under ion impact. Phosphors in the three colours are deposited above the data electrodes and on the dielectric ribs (figure 2). The ribs are generally parallel stripes separating the rows of the panel, as in figure 2, but a recent trend is to close the cell in both directions. For example, plasma displays with 'WAFFLE' ribs [24, 25], or 'DelTA' ribs [26, 27] have been recently built (see photos of the WAFFLE structure in section 3.5, and diagrams of the WAFFLE and DelTA structures in section 6). This improves the collection of VUV photons in a given cell and decreases cross-talk effects. Useful light emitted by phosphors exits PDP through the coplanar electrode face. The discharge also emits visible emission, mainly red–orange light from neon. For improving the primary colour purity, some manufacturers insert capsulated colour filters on the front plate prior to the dielectric layer formation [28] (these filters are not represented in figure 2).

Addressing a cell in the ACM structure is relatively simple (figure 3). A sustaining AC voltage, V_S is constantly applied between the line and column electrodes. The amplitude of the sustaining voltage must be smaller than the breakdown voltage of the discharge cells.

In order to turn a cell to the ON state, a voltage pulse (writing pulse) is applied between the line and column defining the selected cell, as shown in figure 3. The amplitude of this voltage pulse is larger than the breakdown voltage of the cells. A glow discharge forms and is quickly quenched by the charging of the dielectric layers which creates a voltage across the gas gap opposing the voltage across the electrodes. At the end of this 'writing' pulse, the charges on the dielectric surfaces above each electrode are $-Q$ and $+Q$. At the beginning of the next half cycle of the sustaining voltage, the voltage due to the charge on the dielectric surfaces above the dielectrics now adds to the applied voltage and the gas gap voltage (or 'cell voltage') is again above breakdown. A new discharge pulse is initiated. In ACM colour PDPs developed in the 1990s [29, 30], the gas mixtures was Xe(10%)–Ne at pressures between 500 and 600 Torr and the gas gap length 100 μm. With a 500 nm MgO layer above the dielectric surfaces, the sustaining voltage was of the order of 150 V, and the writing voltage between 200 and 250 V. The duration of the current pulses in these conditions is of the order of 20–50 ns (see, e.g. Meunier *et al* [31], Punset *et al* [32]). In the scheme of figure 3, the charges on the dielectric surfaces are $(-Q, +Q)$ after the writing pulse, $(+Q, -Q)$ after the first sustaining pulse, and so on. This corresponds to the ideal case where a steady state regime is reached immediately after the writing pulse. This is possible if the writing voltage is carefully chosen, otherwise the surface charges evolve to this steady state after a few sustaining pulses. Note that the charge transferred during the writing pulse is Q while the charge transferred during the sustaining pulse is $2Q$. Erasing is obtained by applying a voltage pulse smaller than the sustaining voltage and such that the charge transferred during the pulse is Q instead of $2Q$. After the erasing pulse the charges on the surface at the beginning of the next half cycle are zero. The writing, sustaining and erasing pulse voltages can be easily chosen if one knows the 'voltage transfer curve' of the cell. These curves and the stability conditions of the sustaining regime have been analysed by Slottow *et al* [33], Sahni *et al* [34], and Slottow [35] for the ACM structure. We briefly discuss these questions in section 3.2.

Addressing a coplanar cell is more complicated and there are more possible addressing schemes for the ACC structure than for the ACM since the coplanar cell is defined by three electrodes instead of two (see figure 4). When a coplanar cell is in the ON state, a succession of discharge pulses occur between the two coplanar electrodes due to the rectangular AC voltage constantly applied between pairs of coplanar electrodes (the lines of the display). As in the ACM case, the amplitude of this sustaining voltage is below the breakdown voltage of the cell. The third electrode (on the back plate) is called 'data electrode' or 'address electrode' and is used to turn a given cell to the ON state or to the OFF state.

This is illustrated in figure 5 where a first voltage pulse is applied between the A electrode (data electrode) and Y electrode (scan-sustain electrode) and is followed by several sustain pulses. As in the ACM case, the role of the writing pulse is to depose surface charges on the dielectric layers above the sustain electrodes so that the voltage drop in the gas above the sustain electrodes at the beginning of the next half

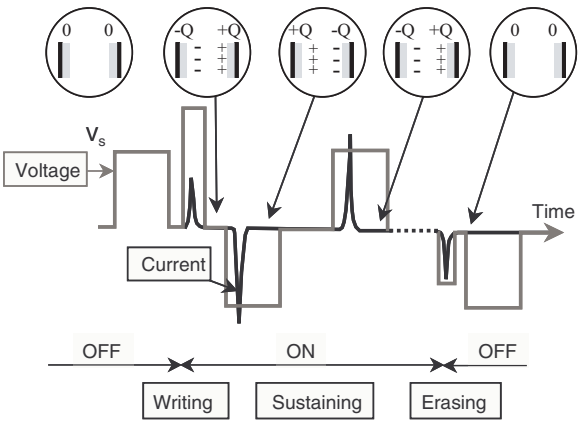

Figure 3. Example of a sequence of writing, sustaining, and erasing pulses in an ACM PDP. The voltage pulses, current pulses, and charges on the dielectric surfaces after each pulse are shown (after Slottow [35]).

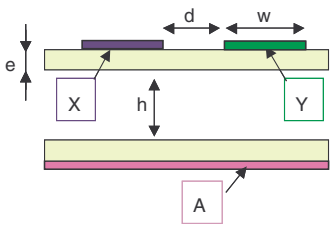

Figure 4. Simplified scheme of a coplanar cell with definitions of notations used in the text. A is the address electrode, X and Y the sustain electrodes, Y the scan electrode.

Downloaded from Plasma.com

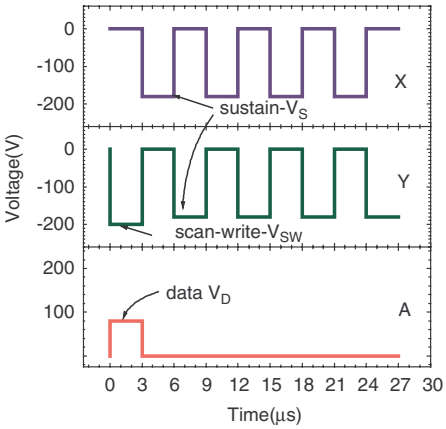

Figure 5. Example of sequence of writing and sustaining voltage pulses in an ACC PDP. The writing voltage pulse is the first one. A scan-write signal is applied to the scan electrode Y (see figure 4) during the writing pulse while a data voltage pulse is applied to the address electrode A. In this example the sustain voltage is −180 V, the scan-write voltage is −200 V, and the data voltage is +80 V.

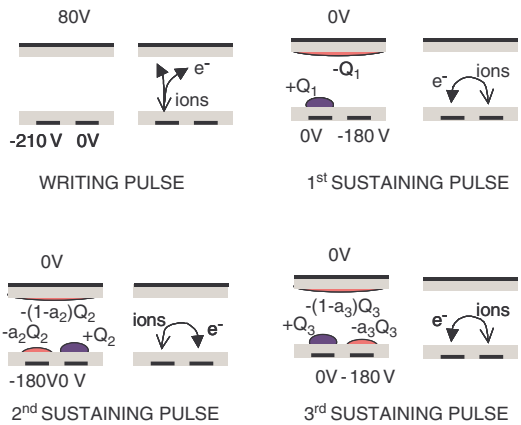

Figure 6. Scheme showing the surface charges above the electrodes at the beginning of the first four voltage pulses of figure 3(*a*), for a coplanar plasma display. Q_k is a charge and a_k a real number. At steady state Q_k and a_k reach constant values, Q and a, which depend on the voltage, gas mixture and cell geometry.

cycle of the sustain voltage becomes larger than the breakdown voltage. The address discharge occurs between the scan-sustain electrode Y and the address electrode A (figures 5 and 6). After this writing pulse, a charge $-Q_1$ lies on the surface above the address electrode, and $+Q_1$ above the scan-sustain electrode (figure 6). The voltage induced by the memory charge $+Q_1$ above the Y electrodes adds to the sustain voltage applied to X at the beginning of the first sustain pulse and a first transient discharge is initiated between X and Y. At steady state, the surface charges above the dielectric layers covering each electrode are $+Q$ and $-aQ$ for the sustain electrodes, and $-(1-a)Q$ for the address electrode, where the a coefficient is in the interval [0, 1]. The value of this coefficient depends on the relative capacitance between the plasma and each electrode, i.e. on the electrode dimensions and positions, and dielectric thickness and permittivity.

Note that the rise time of the writing and sustaining pulses must be short enough so that the current pulse does not occur

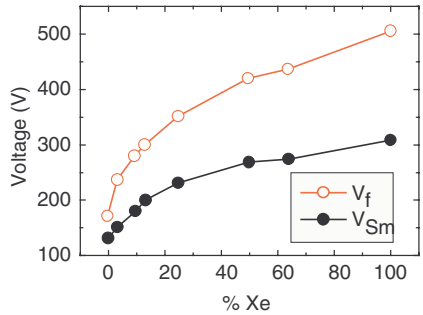

Figure 7. Example of voltage margin as a function of Xe concentration in Ne, in a coplanar PDP cell; the pressure is 450 Torr. (after Gillies and Oversluizen [36]). V_f is the firing voltage and V_{Sm} the minimum sustaining voltage. For sustaining voltages above V_f the cells cannot be turned to the OFF state, and for sustaining voltages below V_{Sm}, a cell cannot be maintained in the ON state. V_f and V_{Sm} depend on the gas mixture, pressure, and cell geometry and dimensions.

during the voltage rise but during the plateau. Practically the rise time is of the order of 200–300 ns.

3.2. Bi-stability, voltage transfer curve and voltage margins

The voltage applied to the electrodes during the sustaining regime must be within two limits that define the voltage margin. Below the lower limit, the discharge cannot be sustained. This lower limit is related to the minimum glow discharge voltage in the DC case (which corresponds to the limit of an infinite capacitance of the dielectric). If the applied voltage is above the upper limit of the voltage margin, all the cells are ON even if they have not been addressed. Since the cells are not perfectly identical, some cells will turn ON before the others when the voltage is above the upper limit of the voltage margin. The upper limit of the voltage margin is the minimum breakdown voltage of all the cells. It is important that the margin be as large as possible and to operate not too close from the limits of the margin (otherwise, cells with slightly different margins will not be ON or OFF for the same voltages). The upper limit of the margin, also called the firing voltage, should however not be too large because the writing voltage increases with the firing voltage. Figure 7 shows an example of measured voltage margin as a function of percentage of xenon in neon [36].

The existence of the voltage margin is a very important property of AC PDPs, and is responsible for the inherent 'memory' of a PDP cell. The basic idea is that once a cell has been turned ON by a writing pulse, it can be sustained at a voltage lower than breakdown (because of the memory charges deposited on the dielectric layers by the writing pulse). Therefore some cells can be in the ON state and others in the OFF state, while the same voltage (sustaining voltage) is applied to all.

The data voltage pulse during addressing must also be within a voltage margin. If the data voltage is too large, the large wall voltage at the end of the addressing pulse may induce a self-erasing current pulse when the data voltage goes back to zero (see, e.g. Nakamura *et al* [37] and the simulations of Punset *et al* [38]). If the data pulse voltage is too low, the cell will not be properly addressed.

The simple diagram of figure 8 shows the voltages and charges in a matrix cell schematically represented by a parallel

Downloaded from Plasma.com

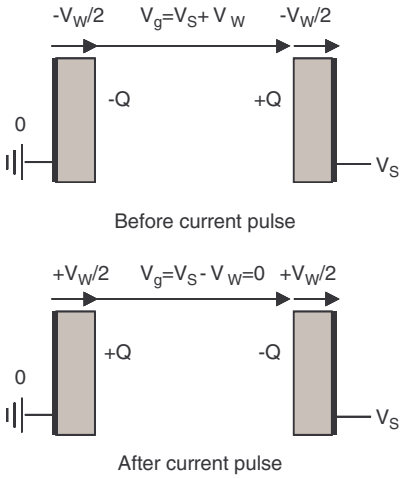

Figure 8. Charges and voltages in a matrix cell before and after a current pulse. At steady state, in a stable sustaining regime one must have $V_W = V_S$ and the voltage across the gas gap is $2V_S$ before the current pulse and 0 after the current pulse. At the beginning of the next voltage pulse, the voltages on the left and right electrodes switch to V_S and 0, respectively, and the voltage across the gas gap is $-2V_S$.

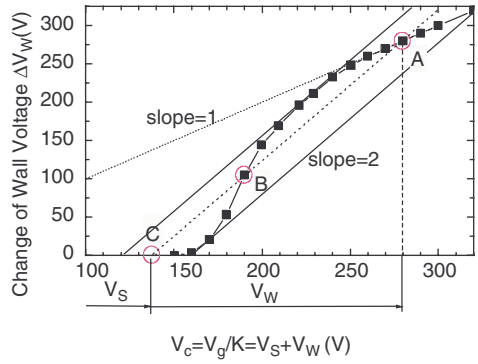

Figure 9. Example of voltage transfer curve (after Slottow [35]); the numerical values are from Meunier *et al* [31]) and are obtained with a one-dimensional model in a Xe(10%)–Ne mixture. A and C are two stable points in the ON and OFF regimes, respectively. The two straight lines of slope 2 define the limit of bi-stability. The intersections of these lines with the horizontal axis corresponds to the minimum and maximum values of V_S in the bistable regime, and define the margin.

plate gas gap between two equal dielectric layers of capacitance C each. The voltages and charges are represented at the beginning and at the end of a voltage pulse in a steady state sustaining regime. The sustaining voltage is V_S. Assume that the voltage drop across the two dielectric layers due to the charges $-Q$ and $+Q$ deposited on the dielectric surfaces by previous discharges is $-V_W$ (i.e. $-V_W/2$ across each). Q and C are related by: $Q = CV_W/2$. In the discussion of the energy per pulse below, we neglect the gas gap capacitance with respect to the dielectric capacitance and V_W is equal to the total voltage drop across the dielectric surfaces. If the gas gap capacitance is not neglected, V_W is slightly different from the total voltage drop V_D (see later, the exact relation between V_W and V_D) across the dielectric layers, which takes into account the electrostatic charges associated with the charging of the dielectric and gap capacitance in series. The voltage across the gas gap before the current pulse is $V_g = V_S + V_W$. If we are in a steady state regime, the charges on the left and right dielectric layers at the end of the current pulse must be $+Q$ and $-Q$, respectively, and the new total voltage drop across the dielectric layers must be $+V_W$ ($+V_W/2$ across each). Under normal operating conditions, the voltage across the gas gap at the end of the pulse, $V_g = V_S - V_W$ should be 0, like in the complete discharge of a capacitor through a resistor. We must therefore have $V_W = V_S$ in stable operating conditions. The change of the voltage across each dielectric layer during the discharge is therefore equal to V_S, and the total change of the wall voltage ΔV_W must be equal to $2V_S$. $\Delta V_W = 2V_S$ is the stability condition. In stable conditions of operations, the voltage across the gap at the beginning of each voltage pulse is $\pm 2V_S$.

The energy dissipated during a discharge pulse is

$$E_{\text{pulse}} = \int_{\text{pulse}} V_S I \, \mathrm{d}t = V_S \int_{\text{pulse}} I \, \mathrm{d}t = 2QV_S = CV_S^2$$

and the charge transferred during the pulse is $\Delta Q = 2Q = CV_S$. Since the equivalent capacitance of the two dielectric layers is $C_D = C/2$, and the gas gap voltage change during the pulse is $2V_S$, the energy per pulse and charge transfer can be written in the usual form:

$$E_{\text{pulse}} = \tfrac{1}{2} C_D [2V_S]^2 \qquad \text{and} \qquad \Delta Q = C_D [2V_S].$$

The concept of voltage transfer curve [33, 35] is very useful to define the stable operating conditions of a PDP cell. An example of voltage transfer curve is shown in figure 9. The voltage transfer curve plots the change of the wall voltage in a given discharge as a function of the initial voltage across the gas gap just before the discharge. The abscissa in figure 9 is actually slightly different from the gas gap voltage if the gas gap capacitance C_g cannot be neglected with respect to the equivalent capacitance of the two dielectric layers $C_D = C/2$. Let $K = C_D/(C_D + C_g)$, and let V_D be the total voltage across the dielectric walls. The exact definitions of the voltages used to plot the voltage transfer curve are (see also the definitions in Johnson *et al* [39], and Meunier *et al* [31]):

$$V_c = \frac{V_g}{K} = V_S + V_W,$$

$$V_W = \frac{V_D}{K} - \frac{V_S(1-K)}{K} = -\frac{Q}{C_D},$$

when C_g is neglected with respect to C_D (i.e. $K \sim 1$), we have $V_c \sim V_g$ and $V_W \sim V_D$, as in the discussion related to figure 8. In typical conditions of AC PDPs, K is between 0.9 and 1. Note that V_W only accounts for the charge deposited on the dielectric by previous pulses while V_D also includes the electrostatic charges associated with the capacitive divider formed by the wall capacitor C_D in series with the gap capacitor C_g.

Slottow and Petty showed that the slope of the voltage transfer curve around the operating point must be less than 2 for stable operations (see the example of figure 9). Weber *et al* [40, 41] defined a slightly different wall voltage input–output curve that plots the output wall voltage as a function of input wall voltage. These curves can be used, for example, to determine the optimal values of the writing, sustaining and erasing voltage pulses of figure 3, or to analyse how the two

Downloaded from Plasma.com

stable states of the cell, the ON or OFF states respond to a perturbation. In the example of figure 9, the operating points for a given value of the sustaining voltage V_S are obtained by plotting a line of slope 2 starting at abscissa V_S, on the horizontal axis [35]. There are three intersections (points A, B, and C) of this line with the voltage transfer curve. It is possible to show that B is not stable. A is the stable point in the ON regime, and C is the stable point in the OFF regime. If the initial wall voltage V_W is in between the abscissa of B and A, it is possible to show that the operating point will move to A, i.e. to the ON state, after a few pulses of the sustaining voltage. If the initial wall voltage V_W is in between the abscissa of C and B, the operating point will move to C, i.e. to the OFF state, after a few pulses of the sustaining voltage. The voltage transfer curve illustrates clearly the concept of bi-stability and allows predicting the response of the cell after a perturbation.

The discussion above was based on a simple, one-dimensional matrix geometry. In a real problem, like in the case of a coplanar electrode configuration, the problem is more complicated because the plasma does not necessarily cover the whole electrode area, and the voltage is not constant along the dielectric surface. However the general ideas of this discussion, i.e. existence of a stability conditions and bi-stability, remain true.

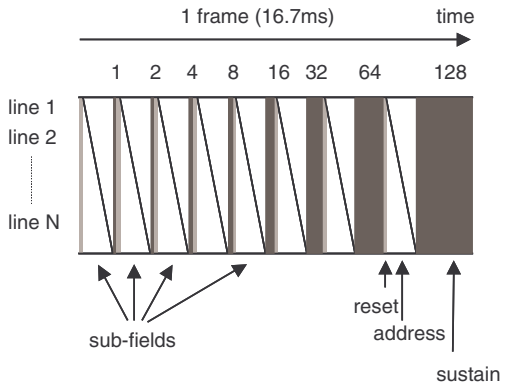

Figure 10. Method of generating 256 grey levels in the ADS method [194]. One 16.7 ms TV-field or frame is divided into eight sub-fields, each containing an address period (with a reset step and an address step), and a sustain period. A given grey level is therefore coded on 8 bits. The reset and address step durations are the same for all sub-fields. The durations of the sustain periods are proportional to 1, 2, 4, . . . , 128. All the cells of a given line are addressed simultaneously. The different lines are addressed sequentially, as indicated by the diagonal lines. In a standard VGA display with 480 lines the total time spent in addressing is about 12 ms while the time spent in sustaining (i.e. time during which the display emits light) is only about 5 ms.

3.3. Panel addressing—grey scale—priming

The principles of addressing and sustaining a coplanar cell have been exposed in section 3.1. The question of addressing becomes much more complicated when one has to deal with addressing and sustaining one or several million cells at a frequency of 60 Hz (60 frames per second) and with the possibility of displaying more than 16 million colours.

Each pixel is composed of three individual cells in the three primary colours. It is possible to display 16.7 millions colours (256 × 256 × 256) if each discharge cell can display 256 intensity levels ('grey scale levels'). This implies the possibility of modulating the light emission intensity of each discharge cell on 256 levels. Obviously this modulation cannot be performed by a modulation of the voltage or current of each discharge pulse. The grey scale is rather obtained by modulating the number of current pulses in a given discharge cell during a TV field (16.7 ms, corresponding to 60 Hz). A binary coding is used to achieve 256 levels. Therefore, a TV field or frame is divided into eight sub-fields where each cell can be sustained for 1, 2, 4, . . . or 128 times a given number of discharge pulses (see figure 10). The 256 possible levels are obtained by turning the cell ON for any combination of the eight sub-fields, as in a binary coding. This allows varying the perceived intensity of the cell to any one of the 256 grey scale levels. During each of the eight sub-fields, it is therefore necessary to reset, address and sustain the cell. The duration of the address period (including a reset step and an address step) is constant, and the duration of the sustain periods in the sub-fields vary in proportion of 1, 2, 4, . . . to 128. One drawback of the binary coding is that the temporal non-uniformity of the light emission scheme (e.g. when changing from the level 127—bits 0–6, to 128—bit level 7) is transformed into a spatial non-uniformity of the light emission pattern on the retina [21, 42]. Motional artefacts such as dynamic false contours may be observed when moving images are displayed on colour plasma displays. Reduction of these disturbances is essential for the picture quality and various methods have been introduced to reduce motional artefacts. These methods are described in Yamaguchi *et al* [21] and Weitbruch *et al* [42].

The driving waveform for one of the sub-fields is displayed in figure 11 in the case of the address display separated (ADS) method proposed by Shinoda [43]. In this method the cells are first prepared during a reset step, then they are addressed (i.e. memory charges are deposited in the cells which need to be ON during this sub-field), and the addressed cells are turned ON during the sustain period (which duration depends on the sub-field). The address and display periods are therefore clearly separated in the ADS method. Many companies use the ADS scheme but other driving methods are possible where some cells may be addressed while other are sustained (AWD, address while display [44]). Within the ADS method, figure 11 shows one possible reset and addressing scheme, but different addressing schemes are possible and are described in different patents.

Addressing clearly consumes a large fraction of the time of a given TV frame since all the lines of the display must be addressed eight times during one frame. Assuming that the duration of each address pulse is τ_{ad}, and that N_{lines} is the number of lines of the panel, the total time T_{ad} necessary to address the display is (neglecting the reset period duration) $T_{ad} = 8N_{lines}\tau_{ad}$. Assuming that the duration of the address pulses, τ_{ad}, is 3 μs, the total addressing time T_{ad} is 11.52 ms for a VGA display (640 rows × 480 lines). This means that only about 5 ms remains for the total sustain duration of a TV frame. It is possible but difficult to use address pulses shorter than 3 μs. This is because, although the current pulse duration is short, of the order or less than 100 ns, the decay time of the plasma, which is mainly controlled by ambipolar diffusion, is of the order of a few microseconds. If the plasma density is

Downloaded from Plasma.com

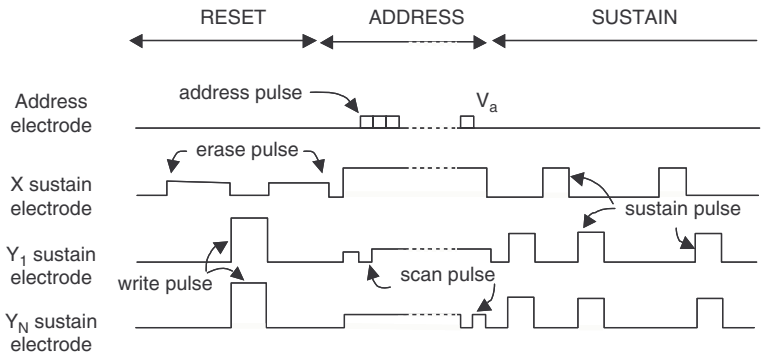

Figure 11. Example of driving waveform (ADS method [43]) for one sub-field of figure 10. The cells are addressed line by line. The same voltage is applied to all the X electrodes. The reset period is used to set all the cells to the same state; in this example the memory charges are first erased, all the cells are then turned ON with a write pulse, and erased again. During the address period an address pulse is sent to the cells of a given line that need to be turned ON while a scan voltage pulse is sent to the Y electrode of each line successively. Memory charges are written on the cell when the scan pulse of a given Y electrode coincides with a pulse on the corresponding address electrode. After the cells of the whole screen have been addressed, the sustain period starts and a discharge occurs in the cells which have been addressed, at twice the frequency of the sustain voltage.

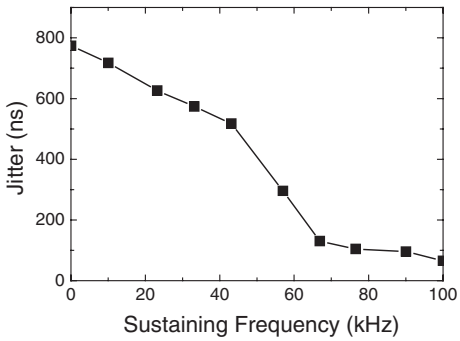

Figure 12. Influence of sustaining frequency on jitter (after Seguin *et al* [195]) in a matrix electrode display (gas gap 130 μm, gas mixture Xe(10%)–Ne, 190 V sustain voltage).

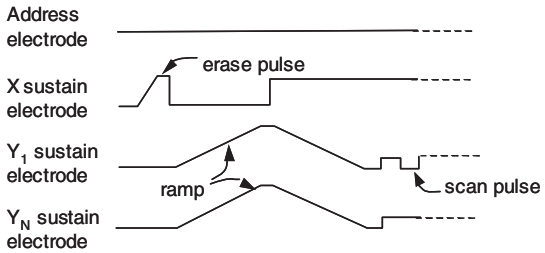

Figure 13. Reset period using ramp voltage to allow efficient priming while keeping good contrast ratio and control of the cell state before addressing (after Weber [50]). If the rise time of the ramp is small enough, the discharge operates in the Townsend regime (dark discharge).

too large when the address pulse is switched off, an unwanted current pulse may partially erase the charges deposited during the address pulse and lead to addressing failure. To ensure successful addressing it is also necessary to keep the delay time to breakdown as short as possible. It is therefore essential to minimize the jitter.

The question of addressing failure due to jitter is important and one of the goals of the reset period is to keep the jitter as low as possible. Jitter is due to statistical lag time [45] of a discharge and is strongly related to the number of available seed electrons in the cell when the address pulse is applied. Seed electrons may be missing in a cell that has not been ON for a long time (black regions of the image).

Figure 12 shows the influence of the sustaining frequency on jitter. It is clear on this picture that a cell which has not been ON for a long time will be difficult to write with a short address pulse. Below 60 kHz, the slope of this curve changes abruptly because the number of charges remaining from the previous pulse becomes too small for pulse lengths smaller than about 10 μs to ensure a fast start of the current pulse. This time is related to the plasma decay due to ambipolar diffusion. Below 60 kHz, the time delay to breakdown becomes more statistical and may depend on other sources of free electrons, e.g. metastable impact on the MgO surface [46, 47], UV photons coming from other cells that are in the ON state, release of electrons from the MgO surface. The curve of figure 12 is strongly modified if neighbour cells are ON, which indicates that UV photons coming from other cells may generate photoelectrons on the MgO surface. The jitter seems to strongly depend on the crystal structure of the MgO layer. The question of the role of the surface on breakdown jitter [48] is rarely discussed in the context of PDPs [49] but may have important implications for driving. The parameters controlling the jitter, i.e. the generation of seed electrons in the cell are very poorly known. Research is needed to study the properties of the MgO surface and its ability to release charges in the gas volume.

The purpose of applying a writing pulse to all the lines during the reset period (figure 11) is to provide enough seed electrons in the cells to decrease current jitter and to ensure that the discharges start in much less than τ_{ad} (e.g. 3 μs) in the cells which are addressed. This is called priming and the writing pulse applied during the reset period is generally a high voltage pulse (several hundreds of V). A consequence of priming with a high voltage pulse is that all the cells of the panels are turned ON at the beginning of each sub-field, i.e. eight times per TV frame, and this generates considerable discharge light. The dark-room contrast ratio (ratio of the luminance of pixel sites in the full intensity state to the luminance of pixel sites in the OFF state) is strongly affected by high-voltage priming because even the cells in the OFF state are turned ON during

Downloaded from Plasma.com

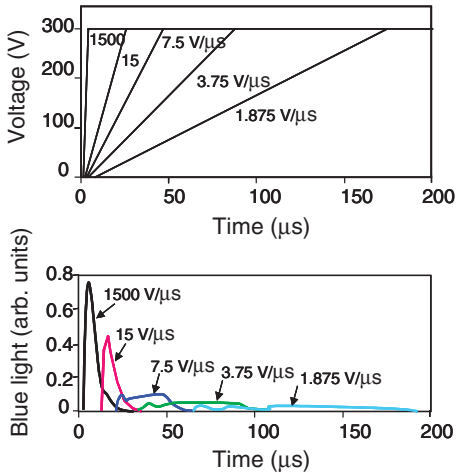

Figure 14. Light output for different ramp waveform (after Weber [41]).

the reset periods. A very nice way of minimizing the amount of light emitted during priming has been introduced by Weber [41, 50]. Instead of applying a high voltage pulse for priming, Weber proposed to replace the voltage pulses in the reset period of figure 11 by the ramp waveforms displayed in figure 13. The ramp voltage slope has to be small enough so that, as soon as the gap voltage reaches breakdown, the discharge stays in a Townsend regime, i.e. the voltage applied between the Y and A electrodes continues to increase while the gas gap voltage stays constant at a value close to the breakdown voltage (due to the continuous, slow charging of the dielectric layers by the dark discharge current). A similar discharge occurs during the negative slope. This allows both a good priming, and a good control of the wall charges (i.e. a well-defined state of the wall charges and voltage) [41]. Figure 13 shows an example of possible reset period consisting of an erase pulse, followed by one positive and one negative ramp voltage. Many variations using ramp voltages are possible and can lead to specific addressing schemes depending on the charges deposited on the cell walls during this period [41]. The analysis of the charge transfer on the different electrodes during the ramp is not easy, and models are very helpful to quantify this aspect [51–53].

Figure 14, from Weber [41] shows the neon light output measured for different slopes of the ramp voltage (the neon light output closely follows the current pulse [54]). The 1500 and the 15 V μs^{-1} ramps show a rapid pulsed type of light output. The 7.5, the 3.75 and the 1.875 V μs^{-1} ramps show a lower peak intensity and correspond to a Townsend discharge where the light output intensity appears to have an amplitude proportional to the ramp rate. This shows that the ramp voltage slope must be a few V μs^{-1}, and the total duration of the ramp voltage is therefore several hundred microseconds.

3.4. Choice of operating conditions—dimension and time consideration—high definition

The operating conditions of a PDP discharge cell are imposed by requirements on the efficiency, screen resolution, addressing speed, sustaining voltage and voltage margin. For a standard VGA 42 in. display, the pixel dimensions are typically 1.08 mm × 1.08 mm (pixel pitch), i.e. the size of one discharge cell is 1.08 mm × 0.36 mm. The height of the cell, i.e. the gas gap is between 0.10 and 0.15 mm.

The requirement of high addressing speed imposes operating at high pressure (the time evolution of the plasma scales as 1 per pressure). On the other hand it is obviously much easier to operate below atmospheric pressure. The pressure in conventional PDPs is between 500 and 600 Torr. At this pressure, the sustaining voltage and voltage margin have reasonable values in xenon–neon mixtures if the coplanar gap length is 60–80 μm (pd product, i.e. product of pressure by coplanar gap length, of the order of 4 Torr cm). The gas gap length (distance between glass substrates) must be large enough so that the discharges take place between coplanar electrodes rather than between one of the coplanar electrodes and the address electrode in the sustaining regime. This imposes a gas gap length more than 100 μm for a 60–80 μm coplanar electrodes gap. On the other hand the gas gap should be less than 200 μm, because the manufacturing of the barrier ribs is difficult or costly for larger gaps. We saw above that the duration of the addressing pulse should be less than 3 μs for a VGA 42 in. display otherwise the time necessary for addressing the whole panel becomes too large with respect to the duration of the TV frame.

The frequency of the voltage waveform in the sustaining regime must be high enough to ensure high luminance, but low enough to make sure that the plasma from the previous pulse has completely decayed at the beginning of a new pulse (otherwise the discharge efficiency decreases [55] and the margin is affected). The ambipolar diffusion time in the conditions of pressure and dimensions of a PDP cell is several microseconds (see, e.g. the model results of Meunier *et al* [31]) so the sustaining voltage frequency cannot be larger that 100–200 kHz under standard conditions.

Assuming that the average power consumption of a display with 1 million pixels ($N_{\text{cell}} = 3$ millions discharge cells) is $P = 1$ kW at $F = 100$ kHz (i.e. 2×10^5 discharge pulses per second), and that the sustain period takes $f = \frac{1}{3}$ of a TV frame, the energy dissipated in each discharge cell per pulse is:

$$E_{\text{pulse}} = \frac{P}{2Ff N_{\text{cell}}} = 5 \times 10^{-9}\,\text{J}.$$

As discussed in section 3.2, the energy per pulse in a DBD with two dielectric layers of capacitance C and a sustaining voltage V_S is equal to CV_S^2. V_S must be within the voltage margin and is imposed by the gas mixture, gap length and secondary emission coefficient. For $V_S = 180$ V, which is typical, the value of the capacitance needed to obtain an energy per pulse of 5 nJ is of the order of $C \sim 0.15$ pF. The charge transferred during one pulse is therefore $\Delta Q = CV_S = E_{\text{pulse}}/V_S \sim 28$ pC (about 2×10^8 elementary charges). Assuming a triangular current pulse of 100 ns duration, this gives a current peak of the order of 0.5 mA which is close to the measurements or model results under typical operating conditions (see the example of figure 15, after Shiga *et al* [56]).

Knowing the required capacitance of the dielectric layer above one sustaining electrode, one can estimate the thickness of the layer. Assuming an electrode area of $A = 300\,\mu\text{m} \times 200\,\mu\text{m}$ in one cell, and taking $C = 0.15$ pF as suggested

Downloaded from Plasma.com

above, the capacitance per unit surface of the dielectric layer must be $C/A = 2.5\,\mu\mathrm{F\,m^{-2}}$. Let ε_r be the relative permittivity of the dielectric, and e its thickness (see figure 4), this gives:

$$\frac{\varepsilon_r \varepsilon_0}{e} \sim 2.5\,\mu\mathrm{F\,m^{-2}} \qquad \text{and therefore} \qquad \frac{\varepsilon_r}{e} \sim 0.3\ (\mu\mathrm{m})^{-1}.$$

This value of ε_r/e is achieved, for example, for typical dielectric materials used in PDPs, with $\varepsilon_r \sim 10$ and $e \sim 30\,\mu$m, or $\varepsilon_r \sim 5$ and $e \sim 15\,\mu$m.

In order to achieve an energy per pulse of 5 nJ, we deduced C for a given, not to high values of V_S. Other considerations may guide the choice of C and V_S, for a given energy per pulse. For example, it is not clear whether, for a given CV_S^2, the efficiency is higher for a larger capacitance and a lower sustaining voltage, or for a smaller capacitance and a larger voltage (assuming that cost of the high voltage drivers is not a problem). Oversluizen *et al* [57, 58] performed experiments, and calculations based on Hagelaar's code [55] which led to the conclusion that operating at higher voltage and lower capacitance is more efficient.

For a 50 in., high-resolution display the pixel pitch would be typically 0.81 mm. The pixel pitch for high definition workstation should however be smaller, typically 0.39 mm × 0.39 mm for a 25 in. diagonal high-definition PDP [59]. This corresponds to a 0.13 mm × 0.39 mm discharge cell and this is close to the lower limit for operating in reasonable conditions of voltage, efficiency and luminance (the experiments of Betsui *et al* [59] show that the operating voltage increases, and the luminance and efficiency decrease with decreasing size of the discharge cell below these values). To overcome this problem, a different arrangement of the coplanar electrodes has been introduced by one of the PDP manufacturers. The principle of the new method, called ALIS [59, 60] for alternate lighting of surfaces, is the following. In contrast with the conventional method, sustain electrodes are arranged at identical intervals and the spaces between them are used as display lines (figure 16). Therefore, the resolution is doubled compared with a standard display having the same number of electrodes. Discharge can be controlled steadily by alternately generating a discharge for the odd and even display lines.

For high resolution displays the conditions on addressing speed become more severe. The maximum addressing time is inversely proportional to the number of lines of the screen (section 3.3) and it becomes difficult to ensure no addressing failure if the address pulse duration must be of the order of 1.5 μs. Dual scan is often used to overcome this problem [28], but the drawback of this method is that the number of electronic drivers for addressing (and the cost of the electronics) must be multiplied by two. In the dual scan method the panel is divided in two parts that are scanned simultaneously. Addressing each line in a time as short as 1.5 μs is however possible and can be achieved by using specific addressing methods [59, 61].

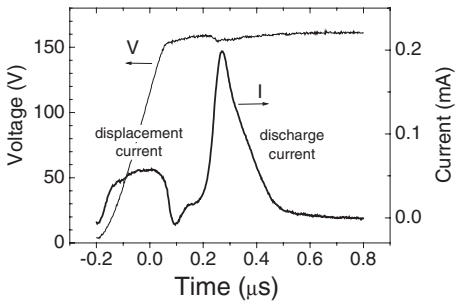

Figure 15. Example of voltage and current waveform (for one discharge cell) measured in the sustaining regime of a coplanar PDP cell (after Shiga *et al* [56]). The current is measured with a whole line ON (640 × 3 cells), and then normalized to get the current per discharge cell (Shiga, personal communication). Since the current is measured on a line with a large number of cells ON, one can expect the current per cell to be slightly shorter and with a higher peak (because of possible time delays between the different pulses).

3.5. *Fabrication process (in brief)*

In this section we give a short overview of the processes and materials involved in the fabrication of PDPs, and on the current research and trends toward cost-reduction.

It is possible to use relatively thin glass substrates in PDPs because the gas pressure is close to atmospheric pressure and barrier ribs can support the front and rear glass substrates. However, the glass plates must withstand the stress arising from mis-matching of thermal expansion coefficients of the glass, barrier ribs, dielectrics, etc and this imposes a lower limit of 3 mm for the glass substrate thickness. Some panels use standard, low cost, float glass. However some thick film processes during the PDP fabrication require baking in a sintering furnace. In these processes the glass substrates is heated up to 600°C, i.e. to temperatures close to the softening point of low cost substrates, which leads to deformation and deterioration of pattern uniformity. Several glass manufacturers have therefore started developing

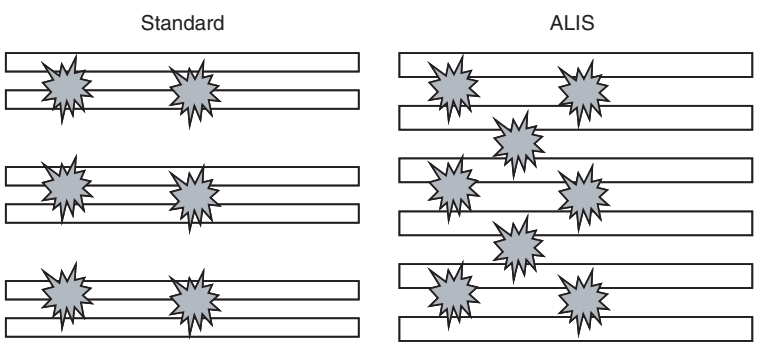

Figure 16. Conventional and ALIS discharge methods (after Betsui *et al* [59]). In the ALIS method, the discharges on the odd and even lines of the display are fired successively in time. The rib structure of the ALIS method is described in section 6.

Downloaded from Plasma.com

special glass substrates with a high strain point and limited deformation.

Sustain electrodes in a PDP consist of indium–tin-oxide (ITO) transparent electrodes and metal bus electrodes (see figure 2). The metal electrodes prevent a voltage drop along the ITO electrodes due to the non-negligible resistivity of the ITO film. Cu has a low resistivity and is well suited for this application but it has poor adhesion to oxide materials so Cr/Cu/Cr structures are often used as bus electrodes. The metal film is deposited by sputtering or printing processes over the entire surface. Photolithography is then used to pattern the electrodes by exposing a photoresist to light through a photomask. Acid etching is then used to remove the unnecessary portion of the metal film. This technology is well controlled but cost reduction is necessary for the metal film deposition process. Another possible technology is to use photosensitive metal (Ag) paste. The entire surface is first coated with the photosensitive paste that is then exposed to light through a photomask to form the electrode patterns. This process is simpler than photolithography and does not require strong acid for etching.

The ITO spreads the plasma over a large surface and allows the light to pass through it. In order to reduce the extra cost associated with the use of ITO electrodes, a new electrode structure has been recently proposed and demonstrated [61, 62]. This 'fence' structure consists in three thin (40 μm), Cr/Cu/Cr horizontal electrodes connected together by vertical shortening bars. The overall width of the fence can be similar to that of ITO electrodes. Like ITO electrodes, the fence structure spreads the plasma and allows a high proportion of light pass through it.

The dielectric layers above electrodes in a PDP must have good dielectric properties, high transparency to visible photons and good thermal expansion matching with soda lime glass substrate. The dielectric layer thickness is between 20 and 40 μm and their formation process uses standard thick film techniques (screen printing followed by drying and firing). Research is directed toward tailoring materials having good dielectric strength and high transparency combined with low firing temperature.

The thin MgO layer (500 nm) is deposited by electron beam evaporation. This is an expensive step because it involves a vacuum process. Ion plating is the second most employed technology after electron beam evaporation, and alternative technologies such as reactive sputtering are also being studied. This step is extremely important since the operating voltage and other discharge characteristics are directly related to the properties of the MgO layer, and each manufacturer certainly has his own recipe for optimizing the MgO film.

Barrier-ribs formation is a process that is specific to PDP fabrication. The challenge is to build up to 1 m long, 100–200 μm high ribs of thickness of the order of 50 μm, with a pitch of about 300 μm (two to three times lower for high definition panels). Currently, two established technologies, sand blasting and screen printing, are dominant, sand blasting being more adapted to higher resolution panels. In the case of screen printing, the substrate is repeatedly coated with paste until the layer reaches the appropriate rib height. Alignment of the different layers is a little bit tricky with this technique. Sandblasting uses fine abrasive powders or glass beads to create the barrier ribs. The thick layer is first coated on the substrate. A photosensitive film is then deposited on the layer and exposed through a photomask. The resulting mask above the coating is then exposed to the blasting of hard fine particles which scrape the unmasked parts of the coating. This process leads to nice barrier ribs with high aspect ratio but is rather lengthy and costly. Other technologies such as press formation, molding of frit glass, blade deforming and grinding are not so widely used or have been proposed more recently [63, 64]. The barrier rib fabrication step is critical to managing manufacturing costs.

Figure 17 shows photographs of the barrier ribs for stripe and WAFFLE ribs structures. The three-colour phosphors are deposited using standard screen-printing techniques. Finally, sealing and exhaust use standard CRT technology processes.

4. PDP performance: efficiency and lifetime issues

As discussed in section 2, efficiency, lifetime, and false contours (and manufacturing costs!) are the main issues of the PDP industry. Efficiency must be improved to lower the electronic drivers cost, lifetime must be increased to reach the consumer's expectations, and false contours associated with the binary coding of the grey levels must be completely eliminated. We will not discuss image quality and false contours in this review and we refer the reader to the recent papers by Yamaguchi *et al* [21] and Weitbruch *et al* [42].

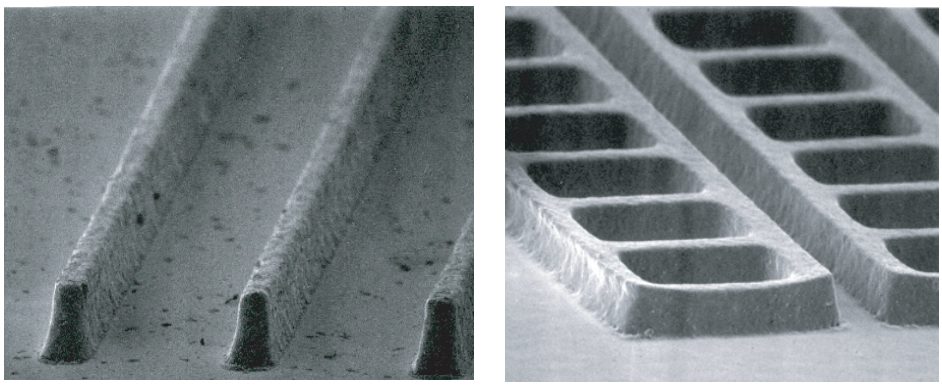

Figure 17. SEM photographs of stripe and WAFFLE rib structures (after Sato *et al* [25]).

Downloaded from Plasma.com

The luminous efficacy of PDPs (ratio of visible radiation or luminous flux to power input) is low, of the order of 1–2 lm W^{-1} in currently produced PDPs. Laboratory prototypes show efficacy of 3 lm W^{-1}, and the goal of the PDP manufacturers is to achieve 5 lm W^{-1}. In this section we analyse the reasons for this very low efficacy compared with what can be achieved in fluorescent lamps. We also discuss some of the lifetime issues.

4.1. General considerations about efficiency

An estimation of the energy balance in a PDP discharge is given in table 1. The first line shows that only 40% of the energy dissipated in the discharge is used for electron heating. Important losses are due to ion heating in the sheath, as demonstrated by the models (see section 5.2). A very simple estimation of the ion heating in the sheath of a dc glow discharge (without positive column) can be obtained by assuming that ionization occurs only in the negative glow and that the negative glow field is zero [65]. These assumptions lead to the result that the fractional power dissipated by ions in the sheath is $P_i/P_T = 1/(1+\gamma)$, where γ is the secondary emission coefficient. About 67% of the total energy is dissipated by ions when $\gamma_i = 0.5$, and 80% when for $\gamma_i = 0.25$. This assumes that the remaining energy is dissipated in the glow by electrons, and that no energy is dissipated in the anode region or in a positive column. This is not true in an AC PDP discharge since a non-negligible part of the electron energy is dissipated in the anode region as discussed in section 5, but the above numbers are very instructive (note that the effective γ_i in a discharge in a PDP mixture is smaller than the γ_i of neon ions since xenon ions are dominant).

Of the energy dissipated by electrons in the discharge ($\rho = 40\%$ of the total electric energy, see table 1), about half or less is used to excite xenon ($\eta_{Xe} \sim 20\%$), the rest being dissipated in ionization of xenon and neon and in neon excitation. Xenon is an efficient UV emitter, and a large part of the energy stored in xenon excitation ends up in VUV photons production ($\eta_{UV}/\eta_{Xe} \sim 75\%$). This is discussed in section 4.2. The energy stored in the xenon excited states is quite efficiently released in VUV energy. A simple estimation based on the cell geometry shows that about 50% of the VUV photons are lost on the front substrate (where there is no phosphor). Improvements in the materials (VUV reflection) could help decrease this important loss. The VUV photons are not efficiently converted (in term of energy conversion) into visible photons by the phosphors even if the quantum efficiency of the phosphors is close to 100% (see section 4.4) because of the large difference ($\sim$ a factor of 3) in energy between the VUV photons ($\sim$147–180 nm) and the visible photons (400–700 nm). UV photons emitted by mercury atoms at 254 nm, as in fluorescent lamps lead to a more efficient energy conversion, but mercury vapour would not be easy to deal with in a PDP. The collection of the visible photons by the user is difficult to estimate precisely. The phosphor must have a good reflectivity for the visible photons (see section 4.4). Table 1 assumes that 60% of the generated visible photons are collected by the user.

The energy balance of table 1 is approximate but helps understand the reasons for the low luminous efficacy of PDPs. It seems possible to improve the collection efficiency of VUV photons and visible photons. It is also clear that the efficiency of the discharge in producing VUV photons is rather low (of the order of 15%) and must be increased. This question is discussed along the rest of this paper.

To better understand the efficiency of electron energy deposition in xenon excitation, it is instructive to look at the results of figure 18(*a*) which shows the fractional energy deposited by electrons in xenon excitation, xenon ionization, neon excitation and neon ionization as a function of the reduced electric field, under uniform field conditions. Although the field is far from being uniform in a PDP discharge, these results give some hints as to the optimum conditions for xenon excitation. We see that when the electric field is increased above several Td (1 Td = 10^{-17} V cm^2), the part of the electron energy that is deposited in xenon excitation decreases, and more energy is put into xenon ionization, neon excitation, and neon ionization. It is therefore clear that the xenon excitation efficiency decreases with increasing electron energy. A simple consequence of this is that the high sheath electric field during the transient PDP discharge is not efficient for xenon excitation and that neon is strongly excited in the sheath (this is confirmed by the models and experiments described in section 5). The lower field of a positive column region would be much more efficient for xenon excitation. Figure 18(*b*) shows that the electron mean energy tends to decrease for increasing xenon percentage in neon. We can therefore expect that mixture with

Table 1. Estimation of the energy balance in a PDP (the energy lost in the electronic drivers is not included). The percentage in the second column is given with respect to the total electric energy dissipated in the cell. The percentage in the third column corresponds to the energy loss between two successive items indicated in the first column.

Energy	%	Loss
Electric energy dissipated in discharge	100	
	↓	60% in ion heating (from models)
Energy dissipated in electron heating	$\rho = 40$	
	↓	50% in xenon ionization, neon excitation and ionization (from models)
Energy dissipated in xenon excitation	$\eta_{Xe} = 20$	
	↓	25% transition loss (e.g. infrared emission), quenching (from models)
Energy dissipated in UV production	$\eta_{UV} = 15$	
	↓	50% VUV photons not collected by phosphors (estimation)
UV energy reaching the phosphors	7.5	
	↓	67% UV to visible photon energy conversion loss (estimation)
Visible photons production	2.5	
	↓	40% visible photons not collected on front face (estimation)
Photons reaching the user	1.5	

Downloaded from Plasma.com

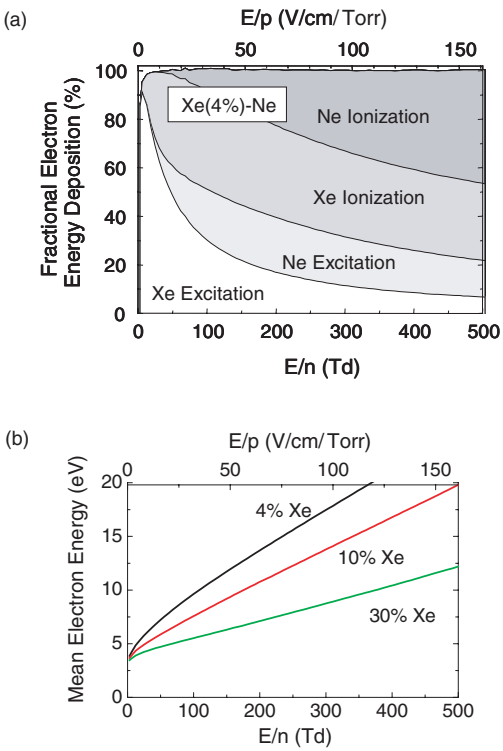

Figure 18. (*a*) Fractional electron energy deposition as a function of reduced electric field in a Xe(10%)–Ne mixture (solution of Boltzmann equation in a uniform electric field [196]); (*b*) mean electron energy as a function of reduced electric field for three Xe–Ne mixture (solution of Boltzmann equation in a uniform electric field [196]). E is the electric field, n is the gas density, and p is the corresponding pressure at 300 K; 1 Td $= 10^{-17}$ V cm^2.

higher xenon contents will be more efficient both because of the larger partial pressure of xenon and because of the lower electron temperature (which compensates for the larger operating voltage).

The results of figure 18 are consistent with the discussion of the PDP efficiency of Suzuki *et al* [66], and with the results of Ikeda *et al* [67].

4.2. *Gas mixture and UV generation*

4.2.1. Gas mixture. The most common mixture used in colour PDP is Xe–Ne, with Xe concentration of the order of 3–10%. Xe is used as VUV emitter and the buffer gas Ne is used to lower the breakdown voltage (because of the large ion induced secondary emission coefficient on MgO, see section 4.3). Increasing the xenon content leads to an increase of the VUV production efficiency, but also to an increase of the breakdown voltage [68]. Systematic and accurate measurements of the Paschen curves [69, 70] under well controlled conditions (i.e. uniform electric field, well characterized MgO layer) in a wide range of rare gas, PDP mixtures, would be very useful and are still missing.

Ternary mixtures of the form $He_xNe_{1-x}Xe(3–5\%)$ have been reported to be more efficient [71] and are used in some commercial PDPs. Noborio *et al* [71] indicate that the optimum helium to neon ratio $x = 0.7$ shows high luminance, high luminous efficiency, low operating voltage and good colour purity. Ne visible emission decreases when He is added and this leads to an improvement of the colour purity. Noborio *et al* also mention that the lifetime of the MgO layer is affected by the relative concentration of He and Ne. The mobility of xenon ions in helium is about three times the mobility of xenon ions in neon, and therefore the concentration of neon in the mixture should not be too small.

Penning ionization (i.e. ionization of xenon atoms by metastable neon atoms) does not have a significant effect on the breakdown voltage in mixtures for colour PDPs because the xenon concentration is relatively large and the electron impact excitation rate of neon is small with respect to the rate of direct xenon ionization. Penning ionization was important in monochrome PDPs where the operating voltage was significantly reduced by adding a small percentage of Ar (∼0.1%) in Ne [72]. As confirmed, e.g. by the calculations of Veronis and Inan [73], adding a small percentage of argon in a Xe–Ne mixture for colour PDPs would not be very helpful for lowering the breakdown voltage. This is however in contradiction with the model results of Min *et al* [74]. The one-dimensional model of Hachiguchi and Tachibana [75] and the zero-dimensional model of Uchida *et al* [76] show that the VUV efficiency should increase in mixtures of Xe–Ne–Ar with larger concentrations of Ar. Also, Uchida *et al* indicate that the use of Ar should reduce the visible emission of neon. Systematic measurements of the efficacy, luminance, minimum sustaining voltages and breakdown voltages in several ternary mixtures involving the rare gases He, Ne, Ar, Kr, Xe have been presented by Gillies and Oversluizen [36]. The authors conclude that while an increase in efficacy and luminance can be achieved in several multicomponent mixtures, it is necessary to examine the associated increase in firing voltage. According to Gillies and Oversluizen, binary Ne_xXe_{1-x} mixtures yield the highest efficacy values at the lowest firing voltages. The efficacy can be increased by a factor of 3 with respect to standard panels by increasing the partial pressure of Xe but this corresponds to a large increase of the firing voltage.

4.2.2. VUV generation in a Xe–Ne mixture. The UV photons in a Xe–Ne discharge are emitted by the resonance and excimer states of xenon. We do not reproduce here the main reactions which take place in a xenon–neon discharge. These reactions and some rates are described in several papers related to PDP discharge models [31, 75, 77–80]. Some of the reaction rates are however poorly known, and studies of the sensitivity of the models to these uncertainties would be useful (an attempt of a sensitivity analysis is presented in the paper by Pitchford *et al* [81]). The main energy transfer processes leading to UV emission are shown in the diagram of figure 19. The lower resonant ($^3P_1$) and metastable ($^3P_2$) states of xenon are shown grouped together in the Xe* level, the 6s′, 6p, 5d and 7s states comprise the Xe** level, and all higher states are included in the Xe*** level. Most of the energy deposited through electron impact excitation of xenon during the current pulse goes into Xe*, either directly or by cascading down from the higher excited states. The $^3P_1$ and $^3P_2$ states are depopulated mainly by UV photon emission from the $^3P_1$ state or by formation of the excimer states Xe_2^* and subsequent UV emission from these excited molecular states. The xenon excimer states are created in the afterglow in three body collisions between the

Downloaded from Plasma.com

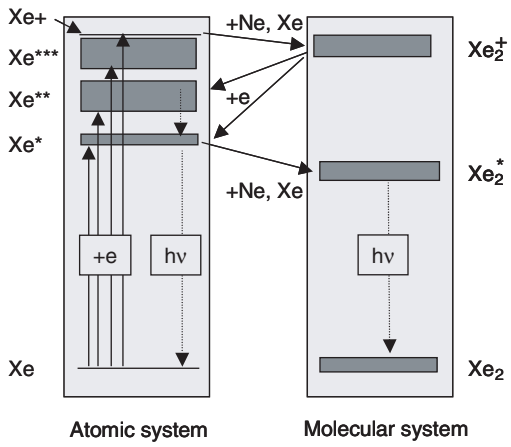

Figure 19. Simplified energy level diagram for atomic and molecular xenon, showing the important excitation and transition processes in PDP conditions.

metastable or resonant states of atomic xenon with two rare gas atoms:

$$Xe^*(^3P_1, {}^3P_2) + Xe + Xe\ (Ne) \rightarrow Xe_2^* + Xe\ (Ne).$$

The efficiency of the energy conversion from xenon excited states to UV photon energy is quite high in the conditions of Xe–Ne PDP discharges. Energy losses in the conversion of atomic excited states to UV photons are due to cascading from the Xe^{**} and Xe^{***} to the Xe^* states (by collisions or radiative de-excitation) and to the energy difference between the metastable or resonance states and the excimer states. The effective lifetime of the resonant state is increased due to trapping (successive emission and re-absorption of the 147 nm photons) and this may lead to excited state and hence VUV photon losses. When the discharge power increases, excited species losses due to stepwise ionization [82, 83] may become important and lead to a saturation [84] of the VUV emission. However recent papers show that under PDP conditions losses due to stepwise ionization of the excited states are not important [57, 85]. This had also been predicted by the models [31, 55, 86], in spite of the uncertainties in the data related to stepwise processes and energy transfer within the atomic xenon system [81, 82]. The consequence is that the discharge efficiency in producing VUV photons closely follows the efficiency in xenon excitation [73, 86]. Typically [31], if the xenon excitation efficiency is 20%, the VUV photon production efficiency is about 15% (see table 1).

Electron recombination with molecular ions (produced by three body collisions) can be an indirect source of creation of xenon resonant and metastable states:

$$Xe^+ + Xe + Xe \rightarrow Xe_2^+ + Xe,$$

$$Xe_2^+ + e \rightarrow Xe^{**} + Xe \rightarrow Xe^*(^3P_1, {}^3P_2) + Xe + h\nu.$$

Okigawa *et al* [87] and Tachibana *et al* [54] report an increase in the metastable density (deduced from laser absorption experiments) after the end of the current pulse, in the afterglow, which can be attributed to recombination. Infrared emission during the afterglow is also an indication of the importance of electron recombination as a source of xenon resonant and metastable states. The time resolved emission measurements of Dekker *et al* [88] show that about 5% and 20% of the total infrared emission occur in the afterglow in a PDP cell in mixtures with 3.5% and 10% xenon in neon, respectively, for a sustain voltage of 180 V. At a higher voltage of 250 V, these percentages increase to about 40% and 60%, respectively. The calculations of Ganter *et al* indicate that about 10% of the total xenon excited state production is due to electron recombination in the afterglow for a 10% xenon–neon mixture. We can conclude that there are large uncertainties in the role of electron recombination on the overall xenon excited state production, but it seems that under standard conditions of relatively low sustaining voltages recombination does not play a major role.

4.3. MgO layer and secondary electron emission

The MgO layer is a key element of PDPs. This thin film (∼500 nm) protects the dielectric layer above the electrodes from sputtering while at the same time yielding a high-ion induced secondary electron emission coefficient (γ_i) for Ne^+. Because of its large secondary electron emission coefficient and good resistance to sputtering, the MgO layer plays an essential role in keeping the operating voltage relatively low and in limiting the damages due to energetic ions. The MgO layer is therefore important both for efficacy and lifetime issues.

The combination of the emissive and protective properties makes MgO quite unique and explains the fact that MgO, which was already used in the 1970s by Uchiike *et al* [89] and others [90, 91], is still used in the PDP industry in spite of many attempts to find materials with better properties. The secondary electron emission coefficient of MgO under xenon ion bombardment is much lower than that of neon ions. Therefore Ne plays an important role in lowering the breakdown voltage in PDP gas mixtures, and this is one of the reasons why neon is used as a buffer gas in PDPs. Bachmann *et al* [92] recently showed that CVD diamond coatings can have (γ_i) values as large as MgO for neon ions and much larger than MgO for xenon ions. Although the feasibility of using CVD diamond coatings in PDPs has not yet been demonstrated, these results are encouraging and show that research for materials with better properties than MgO should continue.

Note that although molecular ions are dominant in the afterglow plasma of a PDP discharge, they do not have time to form in the sheath during the current pulse and the flux of molecular ions to the surface is negligible with respect to the flux of atomic ions [31]. We therefore discuss secondary electron emission and sputtering for atomic ions only.

Secondary electron emission is discussed in this section while section 4.4 deals with the aspects related to sputtering and lifetime.

4.3.1. MgO and other materials with large ion-induced secondary emission coefficient. MgO is not transparent to xenon UV photons, and several groups have been looking for materials with better optical properties with respect to UV transmission. A transparent film would allow coating of the phosphors on the front plate (the front plate phosphors would

Downloaded from Plasma.com

operate in transmission). Note that in the standard design of AC PDPs (figure 2), UV photons hitting the MgO surface above the coplanar electrodes are lost. The corresponding loss in UV in efficiency is therefore close to 50%. Possible candidates for better transmission properties include MgF_2 [93], Al_2O_3 and admixtures of MgO and Al_2O_3 [94]. Elsbergen *et al* [95] have measured secondary emission coefficients for MgO, TiO_2 (good reflective properties for visible photons), mixtures of MgO with Al_2O_3 or CaO. Some of the results of Elsbergen *et al* are shown in figure 20. Some nitrides (AlN) were also studied by Elsbergen *et al* because these materials could in principle exhibit negative electron affinity, but the authors did not succeed in removing O-contaminations by annealing. Park *et al* [96–99] also reports measurements of secondary emission yields for oxides and oxides mixtures such as $Mg_{1-x-y}Sr_x$–Ca_y–O. They report better secondary emission than MgO for some of these mixtures, but this is not confirmed by the measurements of Elsbergen *et al* [95].

The secondary emission yield is also very sensitive to the nature of the surface (amorphous, polycrystalline, single crystal, crystal orientation, etc). Elsbergen *et al* [100] report that the secondary coefficient for (111)-oriented MgO single crystals is substantially larger than for (110) and (100) (see figure 21). They also show that the secondary emission coefficient reaches a constant value only after the surface has been exposed to a plasma for a long enough time. The 'burn time' can be as large as several tens of hours as shown in figure 21. For MgO, the secondary coefficient increases during the burning time but the opposite is true for MgF_2. Other measurements [101–103] made on single MgO crystals also lead to conclusion that the (111) orientation of the MgO crystal has the highest γ_i value.

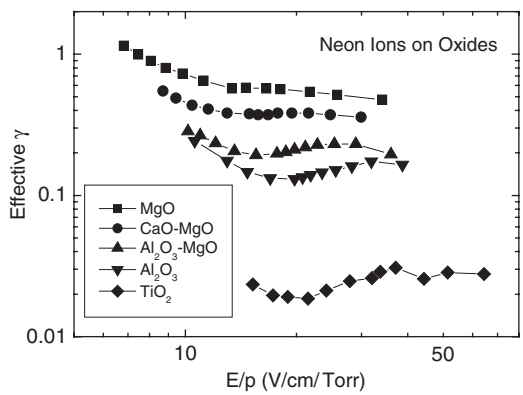

Figure 20. Effective secondary emission coefficients deduced from breakdown measurements by the Lissajous method (see text) for different oxide mixtures in neon (after Elsbergen *et al* [95]).

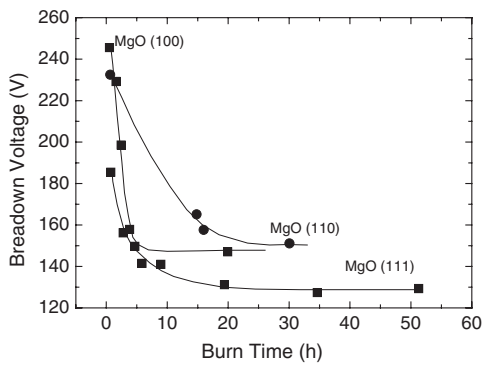

Figure 21. Breakdown voltage of different MgO crystals, for $pd = 7$ Torr cm in Ne, as a function of burn time (i.e. duration of exposure of the MgO substrate to a 30 kHz Ne plasma) (after van Elsbergen *et al* [100]).

4.3.2. Measurements of the secondary emission yield. Although most measurements show similar trends, there is a rather large dispersion in the γ_i measured by different groups. Two different approaches have been used, ion beam measurements, and estimation of γ_i from breakdown voltage measurements (Paschen curves). Ion beam experiments require sophisticated equipment and are not easy to perform because (1) it is difficult to generate low energy ion beams (i.e. of the order of the energy of the ions hitting the MgO surface in PDPs—the mean ion energy on the surface of a PDP cell is between 10 and 20 eV, and fast ions in the tail of the distribution may be up to about 100 eV at most), and (2) MgO is an insulator and the surface potential may vary during the experiment due to charging effects. Ion beam techniques have been used since the 1970s to characterize the secondary electron emission of the protective layer in PDPs [89, 104]. In the early measurements the ion beam energy was too large to provide useful information for PDP conditions. In more recent experiments, measurements with lower ion beam energy, down to 50 eV have been reported [101, 102, 105]. In the energy range around 50 eV the measured γ_i is almost constant or slowly increases with energy which is consistent with Auger neutralization (i.e. γ_i depends on the internal energy of the incident ion, and not on its kinetic energy, see later). However the γ_i reported in several papers for (111) MgO crystals [101, 102], and for polycrystalline MgO [105] are rather low, of the order of 0.05–0.1 for 50 eV neon ions, and about twice larger at 200 eV. Other papers reporting ion beam experiments give larger values of γ_i, ~0.3 for 200 eV helium ions in Kim *et al* [96] and about 0.5 for 300 eV neon ions on MgO in Hirakawa *et al* [94]. The dispersion in the results is therefore very large and it is difficult to draw any quantitative conclusion from these measurements (although comparative studies for different materials or gases performed by the same group are useful).

The second approach is the classical use of breakdown curves or swarm measurements (see the review paper by Phelps and Petrovic [106] and references therein). In this approach one does not obtain the secondary emission coefficient due to ion bombardment only, but an effective secondary electron emission γ_{eff} including the effects of ions, metastable atoms, and photons. The basic idea of using measured breakdown curves or Paschen curves, is that along this curve, the breakdown condition must be satisfied, i.e.:

$$\exp[\alpha d] = 1 + \frac{1}{\gamma_{eff}},$$

where α is the ionization coefficient (supposed to be constant in the gas gap), d the gap length.

For this relation to be valid, the experiment must be performed in uniform field conditions, and corrections must be included for possible non-local effects when the gap length

Downloaded from Plasma.com

is not much larger than the electron energy relaxation length [106]. Knowing the ionization coefficient α and its dependence on electric field E/n (electric field strength over gas density), one can deduce γ_{eff} as a function of E/n. The situation is more complicated when the surface is an insulator, since the gas gap voltage decreases during the pre-breakdown phase due to accumulation of charges on the dielectric surface. A natural way to overcome this problem is to use AC voltage pulses to characterize breakdown. Sahni and Lanza [107] point out that the maximum sustaining voltage is the closest AC panel equivalent to the breakdown voltage. A way to deduce γ_{eff} from AC breakdown measurements is therefore to use a discharge cell similar to a matrix PDP cell, with dielectric layers covered with MgO, but with electrode dimensions sufficiently larger than the distance between electrodes to ensure field uniformity. An AC rectangular voltage is applied between the electrodes and slowly increased until cell ignition is achieved. It is of course important that all remaining charges on the dielectric surface be erased before a new measurement starts which is not the case when the measurements are not performed under AC conditions [108]. The rise time of the AC voltage pulse must be as short as possible so that electron multiplication occurs mainly during the constant voltage step. This method was used in the early studies of PDPs [107, 109, 110]. The question of the influence of the applied frequency (30 kHz in the paper of Aboelfotoh and Lorenzen [109]) of the AC voltage is not discussed, and it is not clear in what frequency range the breakdown results are independent of frequency. More recently, breakdown measurements based on the Lissajous method have been reported [95, 100, 111]. In this method a sinusoidal voltage is applied to the discharge cell in series with a known capacitor. The voltage on the capacitor at each instant is plotted as a function of the applied voltage. This gives a hysteresis curve from which one can deduce the gas gap voltage and thus the breakdown voltage. This technique is valid when the frequency of the applied sinusoidal voltage is small enough so that the discharge never reaches a glow regime but rather stays in the Townsend regime. Similar measurements could also be performed with a ramp AC voltage with a rise time small enough to prevent the discharge transition from the Townsend to the glow regime. In these conditions, as soon as the voltage across the gap reaches the breakdown voltage, the Townsend current charges the dielectric surface in such a way that the gas gap voltage is kept constant and equal to the breakdown voltage. This is reminiscent of Weber's concept of using a ramp voltage for priming (see section 3.3 and Weber [41]). This method seems very attractive but the dependence of the results on the applied frequency (especially for *pd* products larger than 30 Torr cm [111]) is not yet understood and there is a need for a theoretical or modelling clarification of this technique.

The values of the effective secondary electron emission γ_{eff} shown in figure 20 have been deduced from Lissajous breakdown voltage measurements by Elsbergen *et al* [111] in pure neon and for different oxides.

It must be stressed that the methods of estimation of the secondary electron emission based on breakdown curves give an effective coefficient which includes the effect of ion bombardment, but also the effect of metastable and photon impact. Each of these phenomena may be dominant in different parts of the breakdown curve. For example it is known that the contribution of the secondary emission coefficient due to photons is more important for lower E/n or E/p values (i.e. larger *pd* on the breakdown curve). It must also be kept in mind that under some conditions it is possible that the breakdown voltage does not depend on the *pd* product only, but depends separately on pressure and gap length. This has been observed by Sahni and Lanza [112] in the context of monochrome AC PDP (Ne + 0.1%Ar mixture) and was (tentatively) attributed to the fact that atomic and molecular neon ions have different secondary emission coefficients, and that the ratio of molecular to atomic ion flux to the cathode surface increases with pressure.

From the above discussion, we can conclude that there is still a large uncertainty in the γ_{i} and γ_{eff} deduced from ion beam and breakdown experiments, respectively. The different experimental results are in agreement on the fact that the secondary emission coefficients decrease for rare gases in this order: He, Ne, Ar, Kr, Xe, which is consistent with the theory (see later). Also the ion beam experiments as well as the breakdown measurements show that in the case of MgO crystal, the (111) orientation gives the largest γ_{i}. As mentioned above several authors have mentioned that the measured γ reaches a constant value after an exposure to ion bombardment for a long enough duration (more than 10 h for MgO single crystals as reported by Elsbergen *et al* [100], see figure 21). Annealing of the MgO surface is also a necessary process and the typical preparation of MgO for PDPs involves an annealing process at a temperature of the order of 400°C or more (see, e.g. Delplancke-Ogletree *et al* [113] for a study of thermal annealing and effect of exposure to water vapour on the surface structure of single crystal MgO substrate). There are two reaction routes related to water chemisorption on MgO: the formation of hydroxide and of carbonate [97, 114]. Delplancke-Ogletree *et al* [113] report that exposure to humidity modifies the morphology of MgO substrates by the formation of $Mg(OH)_2$ clusters and their results indicate that an MgO crystal cannot be exposed for more than 10 h at 40% or 1.5 h at 80% humidity without undergoing major morphological and chemical transformation.

4.3.3. Theoretical determination of the secondary emission coefficient. The theory of electron emission due to Auger ejection of electrons from metal or semiconductor surfaces is summarized in two classical papers by Hagstrum [115, 116]. Secondary emission by low energy ions depends mainly on the ions potential energy and not on their kinetic energy. In the case of insulating surfaces, the theory shows that the secondary emission yield due to Auger emission is a combination of (1) Auger neutralization, and (2) resonance neutralization followed by Auger de-excitation. In the second case the ion is first transformed into an excited atom when approaching the surface. Even if the probability of the resonance neutralization cannot be easily calculated, it is clear that the total secondary emission coefficient is in between the coefficients corresponding to Auger neutralization and Auger de-excitation. Unlike for metal surfaces, the Auger neutralization secondary electron emission yield does not depend on the surface work function but on the sum of the band gap E_{g} and electron affinity χ of the insulator surface,

Downloaded from Plasma.com

Table 2. Calculated values of the secondary emission coefficient (γ^N through Auger neutralization, and γ^D through resonance neutralization followed by Auger de-excitation) for MgO and BaO assuming a flat band. After Motoyama *et al* [117]. In the case of rare gases and MgO or BaO, $\gamma_i = \gamma^N$, and $\gamma_m = \gamma^D$ where γ_i and γ_m are the secondary electron emissions due to ion and metastable impacts, respectively [117].

Gas	He		Ne		Ar		Kr		Xe	
E_i, E_m (eV)	24.58	19.81	21.56	16.61	15.76	11.55	14.00	9.91	12.13	8.31
γ	γ^N	γ^D	γ^N	γ^D	γ^N	γ^D	γ^N	γ^D	γ^N	γ^D
MgO	0.353	0.406	0.291	0.382	0.032	0.276	0	0.226	0	0.112
BaO	0.376	0.410	0.342	0.388	0.252	0.314	0.211	0.288	0.136	0.251

and on the ion internal energy E_i. More precisely, the emission of electrons by the Auger neutralization process is non-zero when the parameter $G = E_i - 2(E_g + \chi)$ is positive, and increases for increasing G. Therefore, for a given surface, γ_i will increase with increasing E_i, and Xe, Kr, Ar, Ne, He in this order will have increasing γ_i. Note that G is negative for Kr and Xe ions on MgO (if we take, as in Aboelfotoh and Lorenzen [109], a band gap and electron affinity of 6.8 eV and 0.85 eV, respectively) and thus no secondary emission due to Auger neutralization would be expected for Kr and Xe. However the quantity $H = E_{exc} - (E_g + \chi)$ where E_{ex} is the excitation energy, is positive for all the noble gases and secondary emission due to Auger de-excitation should be non-zero even for xenon and krypton.

Aboelfotoh and Lorenzen [109], Motoyama *et al* [117], and Yoon *et al* [118] have used the Hagstrum theory to calculate the ion-induced secondary electron emission yield. The values obtained by Motoyama *et al* [117] for noble gases on MgO and BaO, for the Auger neutralization and Auger de-excitation processes are shown in table 2. The calculations of Yoon *et al* [118] give γ_i values which are slightly larger than those of Motoyama *et al* probably because of different assumptions on the electron escape probability involved in the Auger emission process.

From the results of table 2 we see that the theoretical secondary emission coefficient due to ion impact γ_i is 0.29 for neon ions on MgO and is 0 for xenon ions. The theoretical secondary emission coefficient due to metastable atom impact γ_m is 0.38 for neon and 0.11 for xenon.

Note finally that in a discharge, some of the emitted electrons are backscattered at the cathode. The proportion of backscattered electrons is large for low electric fields and tends to zero for sufficiently large fields [106, 119, 120]. The above theoretical values or ion beam measured values of the secondary electron emission coefficient should therefore be corrected to account for backscattered electrons when used in fluid discharge models.

We can conclude from this section that the theoretical value of the secondary emission coefficient on MgO due to neon ions is generally larger than the value measured in ion beam experiments (0.1–0.3) but lower than values deduced from Paschen measurements (>0.3). The theoretical value of 0 for xenon ions on MgO is quite remarkable since xenon ions are dominant in a PDP discharge and shows that the actual γ_i of xenon ions will strongly depend on the preparation of the MgO surface and on the nature of impurities or dopants included in the layers. The large dispersion of the measured results and the strong dependence of the coefficients on the surface preparation make difficult detailed comparisons between experiments and models of PDP cells.

4.4. MgO sputtering

Energetic ions hitting a surface can lead to the ejection of atoms from the surface. The fast ions also transmit their energy to neutral atoms in the sheath through charge exchange collisions, and the resulting fast neutral atoms can also damage the surface (see McClure [121], Abril *et al* [122], and the calculations in Revel *et al* [123]). Although MgO is quite resistant to sputtering, aging due to sputtering cannot be avoided. The sputtering of MgO may also lead to a contamination of the phosphors (by re-deposition).

In order to estimate the erosion rate or the lifetime of the MgO surface, it is necessary to calculate the energy distribution of ions and neutral atoms hitting the surface above cathode. Several calculations of the ion distribution function at the surface have been reported recently [124–129] (see also Capdeville *et al* [130] for sputtering calculations in Xe–Ne and Xe–Ar mixtures in DC discharges).

The calculated energy distribution functions depend of course on the ion–neutral and neutral–neutral cross-sections, and it is important to use accurate cross-sections. Charge exchange collisions are especially important in limiting the ion energy in the sheath. The cross-sections in Shin *et al* [124] are not discussed (only elastic collisions are mentioned in this paper). Hagelaar *et al* [125] calculated the energy distribution of ions and fast neutral atoms using a Monte Carlo simulation at the moment of maximum ion flux (predicted by a two-dimensional fluid model of a PDP discharge). They propose analytical expressions of the ion distribution that fit well their numerical results. Piscitelli *et al* [127–129] calculated the ion and neutral atoms energy flux distribution with a transient Monte Carlo simulation using the space and time electric field and ionization rates generated by a one-dimensional fluid model. Yoon *et al* [126] used the analytical expressions of Hagelaar *et al* [125] combined with discharge data from a two-dimensional fluid model. From these distributions, and using the sputtering yield obtained with TRIM (a Monte Carlo simulator of the ion–surface interaction [131]), they deduce the lifetime of the MgO layer. All the models agree with the fact that the high energy tail of the xenon ion flux distribution is more populated at lower Xe concentrations while the opposite is true for neon ions, as seen in figure 22. This is because the number of charge exchange collisions between Xe^+ and Xe atoms decrease for decreasing Xe percentage while the number of charge exchange collisions between Ne^+ and Ne increases. The high energy tail of the ion flux distributions is much less populated in the results of Shin *et al* [124] and Hagelaar *et al* [125] than in Piscitelli *et al* [127–129] and Yoon *et al* [126] probably because different cross-sections were used in these papers.

Downloaded from Plasma.com

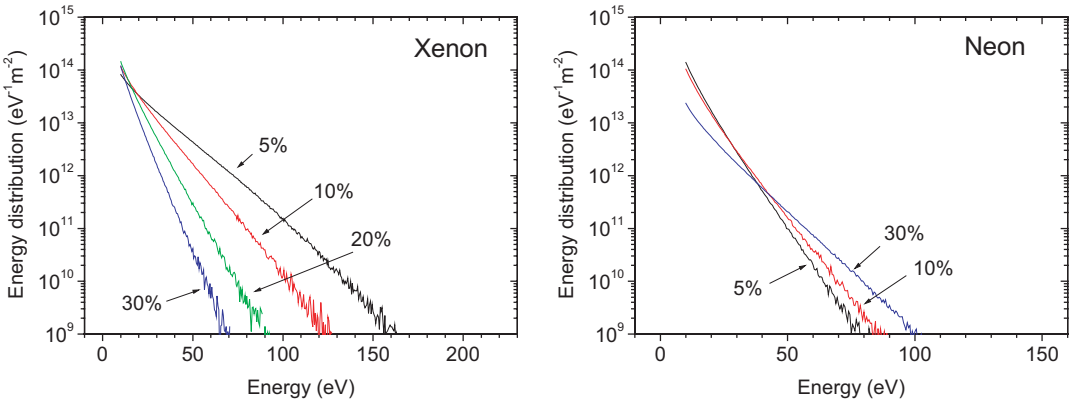

Figure 22. Time integrated flux energy distribution of the ions and fast neutral atoms on the MgO surface above cathode calculated with a Monte Carlo simulation using the space and time electric field and ionization rate from a one-dimensional fluid model (mid-margin, gas gap 100 μm, 500 Torr) (after Piscitelli *et al* [129]). The ion–neutral and neutral–neutral cross-sections used in the simulations are from Phelps *et al* [197].

Even if the ion flux energy distribution can be accurately calculated (if the cross-sections are accurate), it is difficult to estimate the erosion rate (and lifetime) of the MgO layer because it strongly depends on the sputtering yield of the surface near the energy threshold. The sputtering yield can be measured in beam experiments, but measurements at low ion energy are very difficult [132]. The sputtering yield as a function of ion incident energy can be estimated from Monte Carlo simulations of the ion–surface interaction but the uncertainties are large. In the case of Xe–Ne mixtures, the calculated ion energy distributions show that Xe^+ ions are less energetic for larger xenon partial pressure but Ne^+ ions are more energetic. One can therefore expect that xenon ions can cause more damages to the surface at low xenon concentrations while neon ions can cause more damages at higher xenon concentrations (the sputtering threshold of neon ions seems lower that that of neon ions [126], so that even though the neon ion current decreases when increasing the xenon concentration, the contribution of neon ions to sputtering may increase). It is therefore possible that the erosion rate of the MgO surface has a minimum (optimum lifetime) for a given xenon concentration but this needs to be confirmed [129].

4.5. Phosphors

A summary of the demands and achieved performance of PDP phosphors can be found in the recent paper by Bechtel *et al* [133]. In a PDP, phosphors are used to convert VUV light from xenon, into visible light. Phosphor materials must have a high quantum efficiency and low reflectivity for the VUV, and must be highly reflective for visible light. The quantum efficiency at a given wavelength is defined as the ratio of the number of emitted visible quanta to the number of absorbed UV quanta. State of the art PDP phosphors have achieved quantum efficiency in the range from 80% to 95% for xenon UV photons between 147 and 190 nm [133]. The phosphor materials used in PDP applications are $BaMgAl_{10}O_{17} : Eu^{2+}$ (BAM) for blue emission, $Zn_2SiO_4 : Mn^{2+}$ for green emission, and $(Y, Gd)BO_3 : Eu^{3+}$ and $Y_2O_3 : Eu^{3+}$ for red emission. The blue and green phosphors have light output (ratio of the number of emitted visible quanta to the number of *incident* UV quanta, i.e. conversion efficiency including the effect of reflection) above 80% in the xenon VUV range. The red phosphors are a little bit less efficient (the light output of $(Y, Gd)BO_3 : Eu^{3+}$ is close to 80% at 147 nm and about 60% around 173 nm while the light output of $Y_2O_3 : Eu^{3+}$ is of the order of 60% at 147 nm, and closer to 80 around 173 nm). The quantum efficiency, reflectivity and light output of these phosphor materials are plotted as a function of wavelength in Bechtel *et al* [133].

As reported by Bechtel *et al*, the blue emitting BAM phosphor is more vulnerable to panel processing and degradation under panel operation. The quantum efficiency and light output of the BAM phosphor decrease by a factor of 2 for 147 nm photons for an annealing temperature of 1000 K.

Finally, note that the overall efficiency of the photon conversion process (including scattering and absorption of the emitted photons) depends on the size of the phosphor particles. Simulations of the photon conversion process in a PDP cell [133] based on Mie scattering theory show that for a given phosphor layer thickness between 20 and 30 μm, the optimum diameter of the phosphor particles is 1–2 μm.

5. Modelling and diagnostics

Sophisticated modelling and optical diagnostic tools have been developed in the last ten years to study and optimize the discharge plasma in PDPs. In this section we present a non-exhaustive overview of the recent developments of modelling and diagnostic tools.

5.1. PDP models

The first detailed PDP model has been developed by Sahni and Lanza [72] at IBM, for a Ne–Ar (typically 0.1% Ar in Ne), monochrome PDP. The model was one-dimensional and based on fluid equations for electrons, ions, and excited atoms, coupled with Poisson's equation for the electric field. Sahni *et al* demonstrated the capability of such models to successfully simulate the fundamental processes occurring in a PDP cell, from the first principles of gaseous electronics. They showed that the available data (transport coefficients, reaction rates) in Ne–Ar mixtures allowed a detailed understanding of the discharge and relatively accurate predictions of the

Downloaded from Plasma.com

current pulse and voltage-transfer curves. They also showed that the results are very sensitive to the secondary emission coefficient of neon and argon ions on the MgO surface [107, 134]. Meunier *et al* [31] developed a similar one-dimensional model, based on the local field approximation, to study a PDP discharge in a matrix electrode configuration, in Xe–Ne mixtures. A detailed energy balance deduced from this model showed that a large part of the electric energy consumed in the discharge (more than 60% in standard conditions) is dissipated by ions in the sheath. The results showed that about 10% of the electric energy dissipated in the discharge was used to produce UV photons in a Xe(10%)–Ne matrix discharge (100 μm gas gap, 560 Torr, 142 V sustaining voltage). The model also showed that the UV production efficiency can increase with increasing Xe content but that, as well known from experiments (see figure 7), the operating voltage is larger for larger Xe concentrations.

Several papers on one-dimensional models of colour PDP have been published since 1995 [75, 135–139]. After the first two-dimensional models of Uchiike *et al* [140, 141], an increasing number of papers on two-dimensional models have appeared [32, 38, 55, 77, 78, 142–149]. More recently, three-dimensional models of PDP discharges have been developed [150–153]. All the models cited above are fluid models, i.e. the charged particle transport properties are described by average values. A few, more detailed, particle-in-cell Monte Carlo (PIC-MCC) simulations of PDP cells have also been developed recently [154, 155]. These models are time consuming and not well adapted to the relative large collisionality of PDP discharge nor to systematic parametric studies. They may however be very useful to help understanding some detailed properties of electron and ion transport in PDP cells.

Using a two-dimensional fluid model, Boeuf *et al* [32, 38, 142, 143] showed that a non-negligible part of the xenon excitation in a PDP discharge occurs in the anode region, during the spreading of the plasma along the dielectric surface above anode. This feature was later confirmed in optical emission spectroscopy and CCD imaging experiments (see section 5.2), and by all the two-dimensional models. Two-dimensional simulations of the basic operation (writing and sustaining) of a PDP cell in coplanar electrode configurations were described by Boeuf *et al* [68], Punset *et al* [38], and Rauf and Kusher [77, 147]. The ability of the models to simulate the writing and sustaining pulses was demonstrated in these papers.

Figure 23 illustrates the properties of the writing and sustaining discharges as deduced from two-dimensional models. During the writing pulse, breakdown occurs between one of the coplanar electrodes (temporary cathode) and the address electrode. We see the spreading of the plasma above anode and the sheath formation above cathode. Xenon excitation occurs both on the anode and cathode side. The memory charges deposited on the dielectric surfaces during writing allow breakdown between the coplanar electrodes during the sustaining pulse. The glow above the cathode indicates the sheath formation and spreading along the electrode. The plasma spreading along the anode is also accompanied by significant xenon excitation. This excitation is due to the electric field parallel to the surface, induced by the progressive charging of the dielectric surface. Experimental

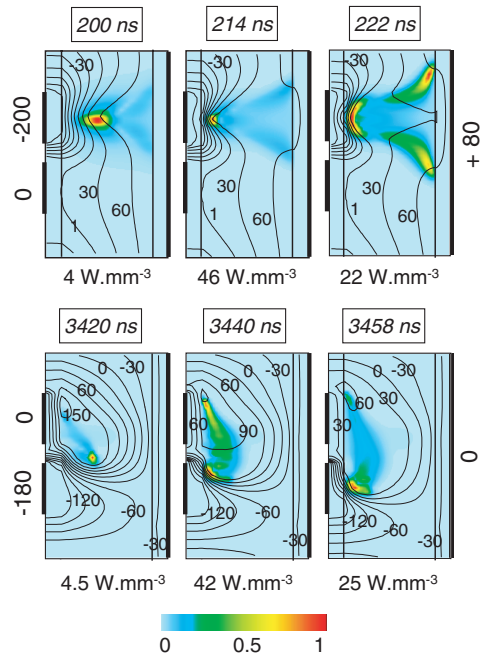

Figure 23. Spatial distribution of power dissipated in xenon excitation (colour) and electric potential (contours) during the writing pulse (top) and the first sustaining pulse (bottom) of a PDP discharge cell (after Punset *et al* [32]). The gas mixture is Xe–Ne (5–95%) at 500 Torr; the cell dimensions are 600 μm × 160 μm (periodic boundary conditions). The applied voltages are shown in figure 5.

results (see section 5.2) confirm this interpretation but show a more complex, striated shape of the emission above the anode.

Rauf and Kushner compared results from a local field model, with results from a hybrid model where a Monte Carlo simulation was used to describe the fast electrons. In agreement with Boeuf *et al* [68], Rauf and Kushner [77] found that the local field approximation did not significantly affect the minimum sustaining voltage, the total current fluence during the discharge, or the accumulated charges on the dielectric surfaces, but that some characteristics such as the discharge initiation time predicted by the local field and Monte Carlo models were different. As in the matrix electrode configuration, the two-dimensional simulations in a coplanar cell showed that an important part of the xenon excitation occurs above the anode. Veronis and Inan [148] also report some differences between results from fluid models using the local field approximation or a local energy approximation.

The calculated data pulse voltage margin in Punset *et al* [38] is in good agreement with the experimental values and these results showed that the two-dimensional model can be a very useful tool for cell optimization. The obvious limitation of the two-dimensional-model is that the cell is supposed to be infinite in the direction perpendicular to the simulation domain. This implies that the width of the address electrode is infinite in the simulation (i.e. the address electrode is not a strip but a plane). The capacitance between the address electrode and the plasma is therefore overestimated by the two-dimensional models, and this has some consequences on the simulated surface charge distribution in the cell, as described by Punset *et al* [38].

Downloaded from Plasma.com

Hagelaar *et al* [156, 157] developed efficient and accurate numerical algorithms for PDP fluid models. They discuss [156] the appropriate boundary conditions that must be used in fluid models where the charged particle flux has a drift-diffusion form. An implicit treatment of the energy equation source term that can considerably speed up the simulation is described by Hagelaar *et al* [157]. More recently, Veronis and Inan [148] presented a similar two-dimensional fluid model of a coplanar discharge and discussed the effect of introducing floating electrodes in the dielectric layers.

One property of the plasma in a PDP cell that is not well described by fluid models is the presence of striations above anode. These striations are clearly seen in optical emission spectroscopy or imaging experiments (see section .2). PIC-MCC models however seem to predict these striations [155,158] (although striations are not mentioned in the paper by Ikeda *et al* [154]), but a clear physical understanding of the mechanisms leading to the formation of striations is still missing.

The models are also very useful because of their ability to give a quantitative estimation of the energy balance in the discharge. One of the important and clear conclusions of all the models cited above is that in typical PDP discharge conditions, a large part of the electrical energy is dissipated in ion heating in the sheaths. The energy is subsequently dissipated through collisions with neutral atoms or when the ion hits the surface. Meunier *et al* [31, 68], Hagelaar *et al* [55] and other authors deduce from their models that more than 60–70% of the input electric energy is dissipated in ion heating. The remaining 30–40% is dissipated into electron heating. The electrons release mainly their energy in xenon or neon excitation and ionization. Roughly speaking about one-half of the electron energy can be dissipated into xenon excitation, the rest being dissipated mainly in xenon and neon ionization and in neon excitation. Therefore about 20% of the total energy dissipated in the discharge can be dissipated in xenon excitation. A large part of this energy (about 80% [31]) is then released into VUV photon energy through cascading and three-body collisions leading to resonant or excimer photon emission.

The two-dimensional model results of Hagelaar *et al* [55] displayed in figure 24 show that between 10% and 16% of the total electric energy dissipated in VUV photon energy in a coplanar discharge under standard conditions (5% Xe, 450 Torr). The efficiency in electron heating (i.e. the part of the total electric energy dissipated in electron heating) is also presented in this figure. The calculations show that the discharge efficiency in producing VUV photons (η_{UV} in figure 24) increases as a function of voltage and saturates at about 300 V for a sustaining voltage frequency of 50 kHz. The electron heating efficiency (ρ in figure 24) increases proportionally to η_{UV}, meaning that the part of the electron energy which is used to produce VUV photons does not significantly change with voltage (η_{UV}, the VUV discharge efficiency, is the product of ρ, the electron heating efficiency, and the efficiency of the conversion of electron energy into VUV photon energy). Hagelaar *et al* [55] report that this increase of efficiency with voltage is consistent with experiments. The simulations of Rauf and Kushner [147] though do not show an increase of efficiency with voltage. It would certainly be very useful to perform benchmark calculations to compare the results from different models in order to identify the real cause for discrepancies (there are large uncertainties in some parameters of the simulation, such as secondary electron emission, ion mobilities in mixtures, or some reaction rates). Another interesting finding of Hagelaar *et al* (see figure 24) is that the efficiency drops if the sustaining voltage frequency is too large. In the 50 kHz case or for lower frequencies the successive pulses are practically independent of each other. For these frequencies only the delay time to breakdown depends on the volume charges (or excited species) remaining from the previous pulse. If the frequency is over a critical value, the delay time may become shorter than the rise time of the voltage pulse. In this case breakdown actually occurs during the voltage rise time and the discharge efficiency decreases.

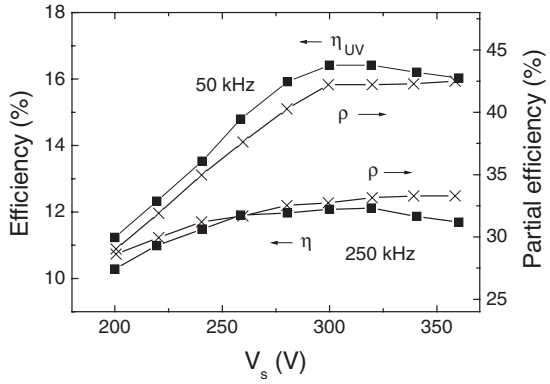

Figure 24. Calculated VUV discharge efficiency as a function of sustaining voltage in a coplanar cell, in a 450 Torr, Xe(5%)–Ne mixture, and for two values of the sustaining frequency. η_{UV} is the discharge efficiency in producing VUV photons (i.e. the ratio of the total energy of the emitted VUV photons divided by the total electric energy dissipated during one pulse). ρ is the percentage of the total energy dissipated in electron heating (the rest, i.e. between 55% and 70% on this graph, being dissipated in ion heating) (after Hagelaar *et al* [55]).

As a general rule the different two-dimensional models show that for a given gas mixture and pressure, there is no spectacular increase of the discharge efficiency when the cell parameters (coplanar electrode gap length, electrode width, dielectric permittivity) are slightly changed around the standard values. The models agree that the discharge efficiency increases with xenon concentration and with pressure, but at the expense of the minimum sustaining voltage, which also increases with Xe concentration and pressure (the operating voltage must be kept as low as possible to keep reasonable electronic drivers costs).

The models can also predict the fraction of VUV photons reaching the phosphors that are emitted by the resonant atomic state of xenon or by the excimer state. The predictions of the two-dimensional model of Hagelaar *et al* are shown in figure 25. We see that about 50% of the VUV photons are emitted by the resonant atomic state for a Xe(5%)–Ne mixture. This percentage drops to about 30% for a Xe(15%)–Ne mixture. This is due to the increase of radiation trapping with increasing xenon partial pressure. The trapping of resonant photons leads to an increase of the production rate of excimer photons through three-body collisions.

Downloaded from Plasma.com

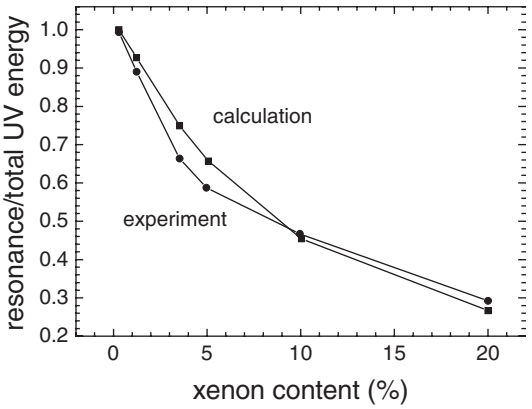

Figure 25. Calculated fraction of the total VUV energy corresponding to resonant photons (147 nm), as a function of xenon percentage (225 V, 450 Torr, 250 kHz) (after Hagelaar *et al* [55]).

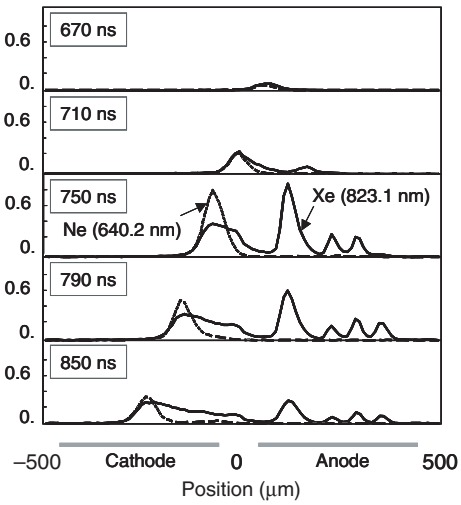

Figure 26. Spatio-temporal emission profiles above the coplanar electrode in a Xe(4%)–Ne mixture at 400 Torr. Neon visible emission (- - - -) mainly occurs above cathode while xenon emission (——) takes place over both cathode and anode. Standing striations are observed above anode (after Yoshioka *et al* [164]).

The results of figure 25 were obtained assuming that the resonance radiation transport can be described with the classical theory of Holstein [159], i.e. using an effective time (or a trapping factor) to account for radiation trapping. A more detailed Monte Carlo simulation of the resonance radiation transport by Hagelaar *et al* [160] showed that this approach is good enough and that the trapping factor estimated from Holstein's theory was in good agreement with the value deduced from the Monte Carlo simulation. The more detailed Monte Carlo approach can also predict the spectrum of the resonant photons leaving the discharge, which can be measured experimentally. As expected, this spectrum exhibits larger wings than a Lorentz profile, and a weaker centre. The simulations of Hagelaar *et al* are in excellent agreement with the measurements [160]. Similar results have also been presented by van Straaten and Kushner [161], Tamida *et al* [162], and Lee *et al* [163].

5.2. Optical spectroscopy and imaging

Detailed optical diagnostics of the plasma in PDP cells have been performed in the last 10 years. These include high resolution, time resolved, optical emission spectroscopy [164], laser absorption techniques [54, 87, 165], imaging using intensified charge-coupled devices (CCD) in the VUV [166–169] and infrared and visible wavelength range [56, 170–173], and, more recently, laser induced fluorescence measurements of the electric field [174] and laser Thomson scattering measurements of the electron temperature and density [175, 176].

In their optical emission spectroscopy measurements, Yoshioka *et al* [164] achieved spatial resolution of 10 μm and temporal resolution of 10 ns. They measured emission lines of atomic He (706.5 nm), Ne (640.2 nm), Xe (823.1, 828.0, 467.1 nm), and ionic Xe (484.4 nm) in Xe–Ne–He mixtures typical of PDPs. The cell dimensions were 1 mm × 0.3 mm × 0.12 mm, the coplanar electrode gap was 100 μm and the electrode width 400 μm. The pressure was varied between 100 and 600 Torr, and the xenon concentration was between 1% and 20%. The cell was driven with rectangular voltage pulses at 10 kHz, in conditions similar to those of a real PDP cell.

Figure 26 shows the distribution of Xe (823.1 nm) and Ne (640.2 nm) above the electrodes (from a top view of the cell, along a line in the middle of the coplanar electrodes) at different times of a discharge pulse in the sustaining regime (400 Torr, Xe(4%)–Ne). We see that light emission first occurs above the anode edge, close to the coplanar gap. After some time an emission peak appears above cathode. This peak corresponds to the negative glow light and moves along the cathode surfaces as the cathode sheath spreads on the dielectric surface above cathode. In the meantime the emission peaks also grow above the anode edge. Three other peaks later appear during the plasma spreading above anode. Note that only xenon emission (823.1 nm) is seen above anode, and no neon light (640.2 nm) is visible, while both xenon and neon lines can be seen above cathode (the neon emission being more peaked). There is no significant neon emission above anode because the electric field responsible for the plasma spreading above anode is too small. This spreading is due to the progressive charging of the dielectric layer that results in a potential gradient parallel to the surface. The corresponding electric field is sufficient to accelerate electrons to energy close to the xenon excitation and ionization thresholds, but is too small for neon excitation. This in excellent qualitative agreement with the prediction of the two-dimensional models.

Yoshioka *et al* [164] showed that the number of striations is related to the gas pressure and xenon content in the mixture (figure 27). Three striations can be seen for the 2% Xe mixture at 400 Torr in figure 27, while four and five striations are seen for 4% and 10% mixtures, respectively.

Several authors [56, 168, 177, 178] have used ICCD cameras to observe infrared and visible emission in a PDP cell. All these papers show the infrared emission above the anode and cathode and the visible neon emission above the cathode only and are in good qualitative agreement with the optical emission measurements described above. The CCD images of Hagiwara *et al* [177] and Cho *et al* [178] exhibit striations above the anode similar to those of figures 26 and 27. ICCD cameras have also been used to measure images of the VUV emission measurements. Such VUV imaging measurements

Downloaded from Plasma.com

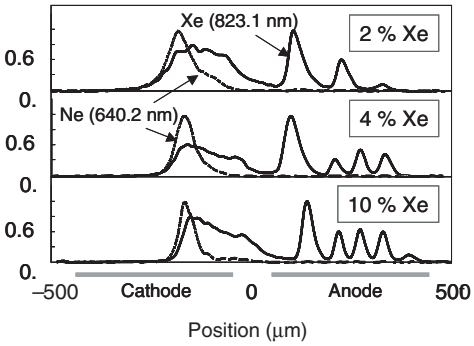

Figure 27. Time integrated emission intensity profiles above the coplanar electrodes for a Xe–Ne mixture at 400 Torr, for three different xenon concentrations (after Yoshioka *et al* [164]).

have been reported by Sawa *et al* [167] and Yoon *et al* [168] and show that photon emission from the resonant line at 147 nm (Xe*) and from the 173 nm continuum (Xe_2^*) are present above both cathode and anode. This is consistent with the infrared emission measurements (the infrared emission is a precursor of the VUV emission since the resonant and metastable states of xenon are populated by radiative decay in the infrared from upper excited states).

Measurements on a 'macroscopic' PDP cell ('macro-cell') have also been reported by Callegari *et al* [171], Ganter *et al* [172, 179], and Ouyang *et al* [180] (see also the paper by Vink *et al* [181]). The macro-cell is a discharge cell whose geometry is similar to that of a real PDP cell, but with dimensions about 100 times larger, and operating at pressure 100 times lower. The macro-cell is a very useful tool for studying PDP discharges because diagnostics are easier than in a real cell, and because the electrode design and cell geometry can be easily modified (and at very low cost). The macro-cell in Callegari *et al* [171], Ganter *et al* [172, 179], and Ouyang *et al* [180] was inserted in a vacuum chamber. A more recent version of the macro-cell has been developed at CPAT in collaboration with Thomson Plasma and is especially convenient since the cell is sealed and the electrodes are outside the cell [182] (the cell walls play the role of the dielectric layers). Many different electrode designs can therefore be tested at very low cost. The images obtained in the macro-cell experiments are strikingly similar to those obtained on real cells (with similar space and time evolution and striations). The velocity of the plasma spreading above cathode was however faster in the macro-cell (1 cm μs^{-1} instead of a few mm μs^{-1}) and this was attributed to a more important influence of photoemission in the macro-cell [173].

Laser absorption techniques provide more quantitative information about the excited states. Okigawa *et al* [87] performed space and time resolved laser absorption measurements of the metastable states of xenon, and showed that striations are present in the metastable atom density, which is consistent with the emission measurements described above. Using a diode laser combined with a microscope, Tachibana *et al* [54, 165] also measured the space and time variations of the metastable ($^3P_2$) and resonant ($^3P_1$) states of xenon in a PDP cell under typical conditions. The address electrode and phosphor layer on the back plate were removed to allow access by the probe laser beam. Figures 28 and 29

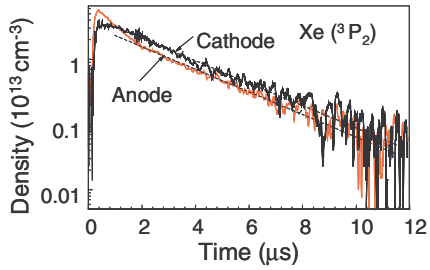

Figure 28. Time evolution of the metastable xenon density above one of the coplanar electrode in a PDP cell (after Tachibana *et al* [54]). Xe(10%)–Ne, 350 Torr, 200 V sustaining voltage, 80 kHz.

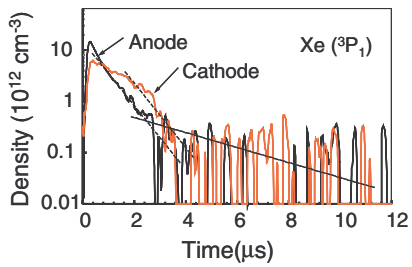

Figure 29. Time evolution of the resonant xenon density above one of the coplanar electrode in a PDP cell (after Tachibana *et al* [54]). Xe(10%)–Ne, 350 Torr, 200 V sustaining voltage, 80 kHz.

show the time evolution of the metastable and resonant state densities, respectively, at a given location above one of the coplanar electrodes (closer to the outer edge of the electrode). The experiments were performed over two half-cycles where the measured side was working either as the temporary cathode or anode. Figure 28 shows that the maximum metastable density is about 5×10^{13} cm^{-3} above anode, and about 3×10^{13} cm^{-3} above cathode (because of the nature of the absorption technique, these values are averaged along the gas gap between the two substrates). Immediately after the current pulse (<200 ns), the metastable xenon density decay is slower above cathode than above anode. Tachibana *et al* [54] attribute this to the possibility of metastable production through electron–ion recombination at the beginning of the afterglow. According to Tachibana *et al*, the faster decay on the anode side could be due to stepwise process or to diffusion in higher mode because of the more localized density distribution above anode. These results also suggest that the plasma density above anode is lower than in the negative glow above cathode. The decay rate later in the afterglow is 2.5 μs above cathode and anode, and this in excellent agreement with the three-body loss rate of the Xe($^3P_2$).

The decay of the resonant state (figure 29) is also slower on the cathode side in the early afterglow. The decay time constant on the anode side is estimated to be 0.37 μs by Tachibana *et al*, and this is in good agreement with an estimation made by the authors and based on the rates for imprisonment of resonant radiation and three-body collisions. The authors also suggest that the slower decay in the late afterglow which can be seen in figure 29 can be due to a population transfer from the $^3P_2$ level to the $^3P_1$ level.

From the space and time resolved measurements of the resonant and metastable densities, Tachibana *et al* deduce the

Downloaded from Plasma.com

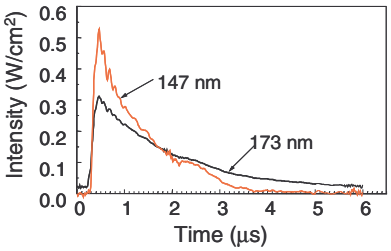

Figure 30. Spatially integrated temporal behaviours of the VUV emissions at 147 and 173 nm estimated from the measured spatio-temporal $Xe(^3P_1)$ and $Xe(^3P_2)$ atom densities (after Tachibana *et al* [54]). Xe(10%)–Ne, 350 Torr, 200 V sustaining voltage, 80 kHz.

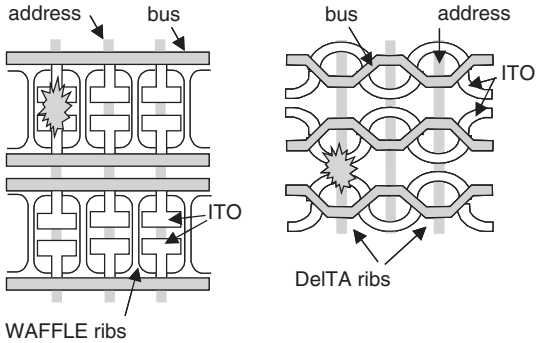

Figure 31. T-shaped electrodes with WAFFLE ribs [24, 25], and meander electrodes with DelTA (Delta Tri-colour Arrangement) ribs [26, 27]. The scales are different; only three full discharge cells are represented in the case of the DelTA structure (these three cells form a triangle or a Delta).

temporal behaviour of the VUV emission at 147 and 173 nm (figure 30). The results show that the contribution of the atomic and molecular species to VUV emission are comparable in these conditions (10% Xe in Ne, total pressure 350 Torr). The authors also show the space distribution of the time integrated VUV emissions at 147 and 173 nm (not shown here, see [54]). The results confirm that the contribution of the anode region to the overall xenon excitation VUV emission is significant in these conditions (about 35% of the total), in agreement with the infrared measurements and with the models. From these results, the authors deduce that the discharge efficiency in producing VUV photons is 5–6% in their conditions, and point out that this is lower but consistent with the calculated 11% of Meunier *et al* [31] (one-dimensional model at 560 Torr), and the calculated 15% of Hagelaar *et al* [55] (two-dimensional model at 450 Torr).

Several authors report direct time resolved measurements of the VUV emission. The measurements of Yoon *et al* [168] for a Xe(1%)–Ne mixture are in qualitative agreement with figure 30 with a slightly shorter duration of the 147 nm emission and a longer duration of the 173 nm emission. The VUV emission measurements of Sawa *et al* [167] in a Xe(4%)–Ne mixture give decay times of the 147 and 173 nm emissions shorter than those of figure 30 by a factor of 2–3, and show that the decay of VUV photon emission is faster above anode. It is difficult to analyse precisely the discrepancies between the different experimental results because the discharge conditions (gas mixture, pressure, voltage) are different. Note that most of the UV emission deduced from the experiments occurs after the current pulse, during the afterglow, in agreement with the models [31, 138, 160, 169].

6. Improvement of PDP efficacy: current research and trends

As discussed in section 4, one of the reasons for the low efficacy of PDP discharges is that a large part of the energy is wasted in ion heating (more than 60%). Also the part of the electron energy that is used for xenon excitation is relatively low (less than 50%). Another decrease in efficiency comes about in the processes leading to the conversion of emitted VUV photons to useful visible photons reaching the user.

The cell design, gas mixture and operating conditions can certainly be optimized to decrease the ion heating and increase the xenon excitation efficiency. An important result from model and experiments (see section 5) is that the xenon excitation and VUV emission above the anode is relatively large in a PDP discharge cell. The energy deposition in this region is much more efficient for xenon excitation than the cathode region (where the sheath field and electron energy are too large for efficient xenon excitation). It is therefore important to try to enhance this aspect, i.e. to look for situations where the relative importance of anode emission would be increased. It has been shown recently that the electrode design can be tailored to some extent to improve the luminous efficacy. For example, it has been shown that the T-shaped electrode geometry of figure 31 leads to slightly higher efficacy [25]. The cell geometry is also an important parameter and using closed cells (e.g. WAFFLE rib structure of figure 17 instead of stripe rib structure) lead to a better efficacy (better collection of VUV photons by the phosphors). The T-shaped electrode structure combined with a WAFFLE rib structure led to an increase of about 40% of the luminous efficacy [25]. The DelTA arrangement of the cells in figure 31, combined with a new 'meander' electrode design [26, 27] has also been shown to improve efficacy. The gas composition is another important parameter. The concentration of xenon in Ne (or Ne–He) used by most companies in commercial products has been generally low (3–5%), but there is a current trend in investigating higher concentrations (between 10% and 15%) [57, 85, 183–185]. The drawback is the increase of operating voltage with increasing xenon partial pressure. Although the Xe–Ne mixture seems well suited for PDP applications, other possible gas mixtures are being investigated.

The T-shape or the meander electrode designs mentioned above and represented in figure 31 are more efficient because they allow a longer extension of the discharge path, as indicated by the CCD images for the T-shaped electrodes [25], and a more efficient VUV collection by the phosphors. The detailed, quantitative reasons for these improvements must be investigated with three-dimensional models. It is however reasonable to think that extending the discharge path allows (1) a more uniform illumination of the phosphors by the VUV photons (reduction of possible saturation effects) and a better collection of the VUV photons with respect to stripe ribs, and (2) operation in a regime closer to a 'positive column' regime

Downloaded from Plasma.com

where a lower field is more suited to efficient xenon excitation (because these geometry tend to force the spreading of the plasma and to increase the discharge path).

A 'positive-column' AC PDP has been recently proposed in a patent by Weber [186]. The positive column AC PDP is characterized by a much longer coplanar gap (about 500 μm). The operating voltage is larger (between 250 and 300 V), but, according to the simulations [128], the xenon excitation efficiency can be increased by a factor of 2. In this configuration the address electrode plays an important role because the coplanar discharge is first triggered by a discharge between one of the coplanar electrodes and the address electrode (this helps lowering the sustaining voltage which would otherwise be much higher). This is illustrated in figure 32 where the address electrode clearly plays the role of an intermediate anode. Models [182] show that the xenon excitation efficiency in this geometry is twice larger than for standard coplanar gaps. The concept of positive column AC PDP looks promising and variations around this concept may lead to a design combining long discharge path and low operating voltage. This could be achieved by using auxiliary electrodes that would help trigger the discharge at low voltage and quickly lead to the formation of a long path discharge.

Recently, the use of radiofrequency (RF) voltages around 50 MHz has been proposed to replace the conventional 100 kHz sustaining voltage [187, 188]. If the frequency of the RF voltage is large enough so that the average amplitude of electron oscillations is less than the gap length, the plasma is efficiently confined by the RF field. In these conditions, the discharge can be sustained at much lower voltages than in the conventional AC PDPs. The ion heating in the sheath is considerably reduced and the electrons excite xenon more efficiently in the lower electric fields. Calculations show that the xenon excitation efficiency can be increased by a factor of 3–4, with respect to AC PDPs [80, 189, 190]. It has been shown that the luminous efficacy can reach 4 lm W^{-1} in RF PDPs, with luminance above 2000 cd m^{-2} [188, 191]. Other technological aspects must however be solved before the RF excitation becomes practical for PDP applications. Among these problems are: efficiency of power coupling to the plasma at these high frequencies, uniformity of the potential along the electrodes for large panels (the wavelength of the RF field is not much larger than the panel dimensions), defining a new addressing scheme for RF PDPs.

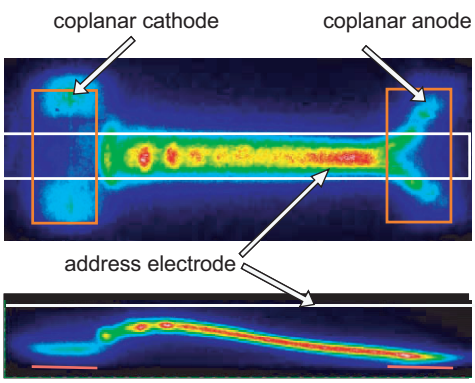

Figure 32. Front view (top) and side view (bottom) of the total, time integrated light emitted by a 'positive column' AC PDP cell obtained with an ICCD camera. Experiments on a macro-cell (dimensions 100 times larger than a real cell, pressure 100 times lower, coplanar gap $d = 5$ cm, coplanar electrode width $w = 1$ cm, gas gap $h = 1$ cm, Xe(5%)–Ne, 5 Torr, sustaining voltage 294 V) (after Ouyang *et al* [182]).

As a general rule, innovations are difficult in PDPs because there are so many constraints (addressing speed, resolution, margin, efficacy, etc) that any positive change on one aspect may have negative consequences on others. In spite of these difficulties, the research for better efficacy and better performances is extremely active as shown by the fast increase of the number of published papers in this domain. There is no doubt that the goal of 5 lm W^{-1} will be reached soon.

7. Conclusion

We have presented in this paper a summary of the physical properties and technological issues of AC PDPs. Emphasis was put on the physics but the technological issues could not be ignored because the needs for a better understanding and control of the basic physical phenomena are dictated by the technological constraints such as high efficacy, high definition, addressing speed, good contrast, etc.

This review shows that the combined effort of engineers and researchers has been extremely fruitful for improving the technology of PDPs, and that the know-how and empirical approach of the manufacturers has benefited from the development of sophisticated diagnostic tools and models. The efficacy of current commercial PDPs is getting close to 2 lm W^{-1}, and 3 lm W^{-1} laboratory prototypes are being announced. The final goal of 5 lm W^{-1} will undoubtedly be reached and the success of the PDP industry will depend only on a reduction of the manufacturing cost, and less on the issue of performance which is constantly improving. The models have shown and the experiments have confirmed that the light emitted by an AC PDP discharge does not originate only from the negative glow region (which is known to be very inefficient for light emission). Significant xenon excitation occurs during the plasma spreading along the dielectric layer above anode. This transient emission is associated with the potential gradient induced along the surface by the progressive charging of the dielectric. Optimization of the electrode design to enhance this anodic emission, research of optimum combinations of gas mixture, dielectric capacitance and applied voltage, and efforts to improve the collection of VUV photons by the phosphors and visible photons through the front face will help improving the efficacy of AC PDPs.

Some questions concerning the physical phenomena occurring in a PDP cell still need more work. These include the plasma–surface interactions: better characterization of the secondary electron emission and better understanding of the parameters controlling the emissive properties of the surface, search for ways to increase secondary emission (possibility of using nanotubes?); phenomena induced by the charging of the surface, mechanisms leading to the release of electrons from the surface; aging of the surface, better characterization of the sputtering yields and estimation of the lifetime from models (the models are becoming sufficiently reliable to predict surface erosion provided that the sputtering yields are known). Some aspects of the charged particle transport and interaction with the electric field also need clarification:

Downloaded from Plasma.com

the mechanisms of the formation of striations are not really understood. The validity of the models must be more carefully checked by performing benchmark model comparisons (as had been done for RF discharge models [192]), and by comparisons with experiments (maybe on simpler, well-defined macro-cell experiments which could be used in the same way as the GEC reference cell for RF reactors [193]. Progresses have been made in the understanding of the energy balance in Xe–Ne mixtures for PDPs, but more systematic studies must be made to better quantify the role of stepwise excitation or ionization, associative ionization, recombination, as mechanisms for losses and creation of excited xenon atoms. It would be also very useful to better assess the potential of the macro-cell as a tool for cell geometry and electrode design optimization. Finally, research on methods of generating the plasma different from the conventional ACC discharge should be pursued.

Acknowledgments

I would like to take this opportunity to gratefully acknowledge the contributions of many colleagues over the years to the ongoing PDP project at the CPAT in Toulouse, which made this review possible. Many graduate students, A Rabehi, J Meunier, A Hirech, C Punset, S Cany, Th Callegari, R Ganter, D Piscitelli, B Caillier, postdocs and vistors, J Ouyang, T Shiga, G Hagelaar, and other colleagues, L C Pitchford, Th Callegari, Ph Belenguer, J Galy, H Brunet, Ph Guillot, N Sadeghi, have contributed to the work leading to the review presented here. I also would like to thank L C Pitchford in particular for carefully reading the manuscript and for useful remarks. S Mikoshiba and T Shinoda are gratefully acknowledged for their thoughtful suggestions and comments. Several colleagues sent digital copies of their published figures for reproduction in this review, and I thank them for their contribution. I would also like to acknowledge my industrial colleagues for numerous useful discussions, in particular, L Tessier and H Doyeux from Thomson Plasma and J Kang from LG Electronics. Continuous support over the years from H Doyeux and J Deschamps of Thomson Plasma and J P Budin of Thomson Multimedia is gratefully acknowledged. Finally, the meetings of the SID (Society for Information Display) have provided occasions for many interesting and enlightening discussions with other industrial and academic colleagues in this field, many of them with more expertise than myself in certain areas discussed in this paper. In this context, I would like to cite in particular L Weber and H Uchiike.

References

[1] Mentley D E and Stanford Ressources 2001 *Bay Area Chapter—Society for Information Display—After-work Monthly Seminar Series* http://www.ba-sid.org/Archives/2001/BA-SID%20Sept-01-dem-sr.pdf
[2] Poor A 2002 *Display Europe* **20**
[3] Weston G F 1975 *J. Phys.* E **8** 981
[4] Bitzer D L and Slottow H G 1966 *AFIPS Conf. Proc.* vol 29, p 541
[5] Slottow H G 1976 *IEEE Trans. Electron Devices* **ED-23** 760
[6] Weber L F 1985 *Flat Panel Displays and CRTs* vol, chapter 10, ed L E Tannas Jr (New York: van Nostrand Reinhold) p 332
[7] Michel J P 1989 *Display Engineering* ed D Bosman (Amsterdam: North Holland) p 185
[8] Sobel A 1991 *IEEE Trans. Plasma Sci.* **19** 1033
[9] Shinoda T and Niinuma A 1984 *SID*, *84* 172
[10] Shinoda T, Wakitani M, Nanto T, Yoshikawa K, Ohtsuka A and Hirose T 1993 *SID*, *93* 161
[11] Shinoda T, Wakitani M, Nanto T, Kurai T, Awaji N and Suzuki M 1991 *SID*, *91* 724
[12] Dick G W and Biazzo M R 1976 *IEEE Trans. Electron Devices* **ED-23** 429
[13] Dick G W and Biazzo M R 1979 *IEEE Trans. Electron Devices* **ED-26** 1168
[14] Holz G E 1972 *SID*, *72* 36
[15] Murakami H and Toyonaga R 1982 *IEEE Trans. Electron Devices* **29** 988
[16] Yamamoto T, Kuriyama T, Seki M, Katoh T, Murakami H, Shimada K and Ishiga H 1993 *SID*, *93* 165
[17] Kamegaya T, Matsuzaki H and Yokozawa M 1978 *IEEE Trans. Electron Devices* **ED-25** 1094
[18] Mikoshiba S, Shinada S, Takano H and Fukushima M 1979 *IEEE Trans. Electron Devices* **ED-26** 1177
[19] Mikoshiba S, Shinada S and Shirai S 1985 *J. Appl. Phys.* **58** 3720
[20] Kariya K, Kanazawa Y and Hirose T 2002 *J. SID* **10** 11
[21] Yamaguchi T, Toda K, Zhu Y W, Shiga T, Mikoshiba S, Ueda T, Kariya K and Shinoda T 1999 *J. SID* **7** 227
[22] Kogelschatz U, Eliasson B and Egli W 1999 *Pure Appl. Chem.* **71** 1819
[23] Tanaka Y 1955 *J. Opt. Soc. Am.* **45** 710
[24] Komaki T, Tanigushi H and Amemyia K 1999 *Int. Display Workshop* **IDW'99** 587
[25] Sato Y, Amemiya K and Uchidoi M 2002 *J. SID* **10** 17
[26] Toyoda O, Kosaka F N T, Tokai A, Inoue H and Betsui K 1999 *Int. Display Workshop* **IDW'99** 599
[27] Hashimoto Y, Seo Y, Toyoda O, Betsui K, Kosaka F N T, Tokai A and Namiki F 2002 *J. SID* **10** 151
[28] Sano K, Nakamura T, Numomura K, Konishi Z, Usui M, Tanaka A, Yoshida Z, Yamada H, Oida O and Fujimura R 1998 *SID*, *98* 275
[29] Deschamps J and Doyeux H 1997 *Phys. World* 39
[30] Doyeux H 2000 *SID*, *00* 212
[31] Meunier J, Belenguer P and Boeuf J P 1995 *J. Appl. Phys.* **78** 731
[32] Punset C, Boeuf J P and Pitchford L C 1998 *J. Appl. Phys.* **83** 1884
[33] Slottow H G and Petty W D 1971 *IEEE Trans. Electron Devices* **ED-18** 650
[34] Sahni O and Lanza C 1977 *IEEE Trans. Electron Devices* **ED-24** 853
[35] Slottow H G 1977 *IEEE Trans. Electron Devices* **ED-24** 848
[36] Gillies M F and Oversluizen G 2002 *J. Appl. Phys.* **31** 6315
[37] Nakamura T, Iseki K, Sano Y and Nunomura K 1995 *SID*, *95* 807
[38] Punset C, Cany S and Boeuf J P 1999 *J. Appl. Phys.* **86** 124
[39] Johnson R J, Bitzer D L and Slottow G H 1971 *IEEE Trans. Electron Devices* **ED-18** 642
[40] Weber L F, Warren K W and Weikart G S 1986 *IEEE Trans. Electron Devices* **ED-33** 1159
[41] Weber L 1998 *Proc. Asia Display* **98** 15
[42] Weitbruch S, Zwing R and Correa C 2001 *J. SID* **9** 279
[43] Yoshikawa K, Kanazawa Y, Wakitani W, Shinoda T and Ohtsuka A 1992 *Japan. Display* **92** 605
[44] Seki S, Ishii M, Shiga T, Igarashi K and Mikoshiba S 2000 *SID*, *00* 714
[45] Pejovic M M, Ristic G S and Karamarkovic J P 2002 *J. Phys. D: Appl. Phys.* **35** R91
[46] Ishii M, Takeda Y, Shiga T, Igarashi K and Mikoshiba S 2000 *J. SID* **8** 217
[47] Röpcke J and Zahn R J 1990 *Contrib. Plasma Phys.* **30** 511
[48] Kudrle V, LeDc E and Fitaire M 2049 *J. Phys. D: Appl. Phys.* **32** 2049

Downloaded from Plasma.com

[49] Röpcke J, Zimdahl T, Schlott D and Glaefeke H 1990 *Contrib. Plasma Phys.* **30** 679
[50] Weber L 1998 *US Patent* 5745086
[51] Nagorny V, Drallos P and Weber L 2000 *SID*, *00* 114
[52] Kim J K, Chung W J, Seo J H and Whang K W 2001 *KIDS J. Inform. Display* **2** 24
[53] Boeuf J P, Kang J, Caillier B, Callegari T, Ganter R, Ouyang J, Pitchford L C and Punset C 2001 *Int. Meeting Inform. Display* **IMID'01** 113
[54] Tachibana K, Feng S and Sakai T 2000 *J. Appl. Phys.* **88** 4967
[55] Hagelaar G J M, Klein M H, Snijkers R J M and Kroesen G M W 2001 *J. Appl. Phys.* **86** 2033
[56] Shiga T, Igarashi K and Mikoshiba S 1998 *Int. Display Workshop* **IDW'98** 487
[57] Oversluizen G, Klein M, deZwart S, vanHeusden S and Dekker T 2000 *Appl. Phys. Lett.* **77** 948
[58] Oversluizen G, deZwart S, Dekker T and Gillies M F 2002 *SID*, *02* 848
[59] Betsui K, Namiki F, Kanazawa Y and Inoue H 1999 *FUJITSU Sci. Tech. J.* **35** 229
[60] Kariya K, Kanazawa Y and Hirose T 2002 *J. SID* **10** 11
[61] Weber L 2000 *SID*, *00* 402
[62] Schindler W C 1999 *Int. Display Workshop* **IDW'99** 735
[63] Kaelber T, Walther M, Vos M, Julius P, Pallhorn S, Buzak T S, Ilcisin K J and Hinchliffe R D 2000 *SID*, *00* 487
[64] Kuromitsu Y, Toriumi M, Toyoda S and Kanda Y 1999 *SID*, *99* 10
[65] Ganter R, Callegari T, Pitchford L C and Boeuf J P 2002 *Appl. Surf. Sci.* **192** 2999
[66] Suzuki K, Kawanami Y, Ho S, Uemura N, Yajima Y, Kouchi N and Hatano Y 2000 *J. Appl. Phys.* **88** 5605
[67] Ikeda Y, Verboncoeur J P, Christenson P J and Birdsall C K 1999 *J. Appl. Phys.* **86** 2431
[68] Boeuf J P, Punset C, Hirech A and Doyeux H 1997 *J. Phys. IV France* **7** C4-3
[69] Postel O B and Capelli M A 2000 *Appl. Phys. Lett.* **76** 544
[70] Postel O B and Capelli M A 2001 *J. Appl. Phys.* **89** 4719
[71] Noborio M, Yoshioka T, Sano Y and Nunomura K 1994 *SID*, *94* 727
[72] Sahni O, Lanza C and Howard W E 1978 *J. Appl. Phys.* **49** 2365
[73] Veronis G, Inan U S and Pasko V P 2000 *IEEE Trans. Plasma Sci.* **28** 1271
[74] Min B K, Lee S H and Park H G 2000 *J. Vac. Sci. Technol.* A **18** 349
[75] Hachigushi S and Tachibana K 2001 *Japan. J. Appl. Phys.* **40** 1448
[76] Uchida S, Sugawara H, Sakai Y, Watanabe T and Hong B H 2001 *J. Phys. D: Appl. Phys.* **34** 947
[77] Rauf S and Kushner M J 1999 *J. Appl. Phys.* **85** 3460
[78] Seo J H, Chung W J, Yoon C K, Kim J K and Whang K W 2001 *IEEE Trans. Plasma Sci.* **29** 824
[79] Uchida S, Sugawara H, Sakai Y, Watanabe T and Hong B H 2000 *J. Phys. D: Appl. Phys.* **33** 62
[80] Kurihara M and Makabe T 2001 *J. Appl. Phys.* **89** 7756
[81] Pitchford L C, Kang J, Punset C and Boeuf J P 2002 *J. Appl. Phys.* **92** 6990
[82] Sommerer T J 1996 *J. Phys. D: Appl. Phys.* **29** 769
[83] Sommerer T J and Doughty D A 1998 *J. Phys. D: Appl. Phys.* **31** 2803
[84] Mikoshiba S and Murayama S 1980 *Appl. Phys. Lett.* **37** 529
[85] Oversluizen G, Klein M, deZwart S, vanHeusden S and Dekker T 2002 *J. Appl. Phys.* **91** 2403
[86] Boeuf J P, Callegari T, Punset C and Ganter R 1998 *Proc. Asia Display'98* p 209
[87] Okigawa A, Yoshioka T and Toki K 1999 *SID*, *99* 276
[88] Dekker T, Oversluizen G, Gillies M F and Zwart S d 2001 *Int. Display Workshop* **IDW'01** 917
[89] Uchiike H, Miura K, Nakayama N, Shinoda T and Fukushima Y 1976 *IEEE Trans. Electron Devices* **ED-23** 1211
[90] Byrum B W Jr 1975 *IEEE Trans. Electron Devices* **ED-22** 685
[91] Urade T, Iemori T, Osawa M, Nakayama N and Morita I 1976 *IEEE Trans. Electron Devices* **ED-23** 313
[92] Bachmann P K, Elsbergen V v, Wiechert D U, Zhong G and Robertson J 2001 *Diamond Relat. Mater.* **10** 809
[93] Sasaki T, Harano Y, Kawai Y, Kamiya M, Uchiike H and Lin H 1996 *SID*, *96* 283
[94] Hirakawa T, Uchiike H and Zhang S 2000 *Int. Display Workshop* **IDW'00** 691
[95] Elsbergen V v, Backmann P K and McGrath C 2001 *Int. Display Workshop* **IDW'01** 937
[96] Kim R, Kim Y, Cho J and Park J W 2000 *J. Vac. Sci. Technol.* A **18** 2493
[97] Kim R, Kim Y and Park J W 2000 *Thin Solid Films* **376** 183
[98] Cho J, Kim R, Lee K W, Yeom G Y, Kim J Y and Park J W 1999 *Thin Solid Films* **350** 173
[99] Cho J and Park J W 2000 *J. Vac. Sci. Technol.* A **18** 329
[100] Elsbergen V v, Bachmann P K and Zhong G 2000 *Int. Display Workshop* **IDW'00** 687
[101] Choi E H, Oh H J, Kim Y G, Ko J J, Lim J Y, Kim J G, Kim D I, Cho G and Kang S O 1998 *Japan. J. Appl. Phys.* **37** 7015
[102] Kim D I, Lim J Y, Kim Y G, Ko J J, Lee C W, Cho G S and Choi E H 2000 *Japan. J. Appl. Phys.* **39** 1890
[103] Ishimoto M, Hidaka S and Betsui K 1999 *SID*, *99* 552
[104] Chou N J 1977 *J. Vac. Sci. Technol.* **14** 307
[105] Moon K S, Lee J and Whang K W 1999 *J. Appl. Phys.* **86** 4049
[106] Phelps A V and Petrovic Z L 1999 *Plasma Sources Sci. Technol.* **8** R21
[107] Sahni O and Lanza C 1976 *J. Appl. Phys.* **47** 5107
[108] Auday G, Guillot P and Galy J 2000 *J. Appl. Phys.* **88** 4871
[109] Aboelfotoh M O and Lorenzen J A 1977 *J. Appl. Phys.* **48** 4754
[110] O'Hanlon J F 1978 *IBM J. Res. Dev.* **22** 626
[111] Elsbergen V v, Bachmann P K and Juestel T 2000 *SID*, *00* 220
[112] Sahni O and Lanza C 1981 *J. Appl. Phys.* **52** 196
[113] Delplancke-Ogletree M P, Ye M, Winand R, Marneffe J F d and Deltour R 1998 *J. Mater. Res.* **14** 2133
[114] Holt S A, Jones C F, Watson G S, Crossley A, Johnston C, Sofield C and Myhra S 1997 *Thin Solid Films* **292** 96
[115] Hagstrum H D 1956 *Phys. Rev.* **104** 672
[116] Hagstrum H D 1961 *Phys. Rev.* **122** 83
[117] Motoyama Y, Matsuzaki H and Murakami H 2001 *IEEE Trans. Electron Devices* **48** 1568
[118] Yoon S J, Lee I, lee J W and Oh B 2001 *Japan. J. Appl. Phys.* **40** 809
[119] Nagorny V P and Drallos P J 1997 *Plasma Sources Sci. Technol.* **6** 212
[120] Murakami Y, Matsuzaki H and Ikuta N 2001 *Japan. J. Appl. Phys.* **40** 3382
[121] McClure G W 1961 *Phys. Rev.* **124** 969
[122] Abril I, Gras-Marti A and Valles-Abarca J A 1983 *Phys. Rev.* A **28** 3677
[123] Revel I, Pitchford L C and Boeuf J P 2000 *J. Appl. Phys.* **88** 2234
[124] Shin Y K, Lee J K, Shon C H and Kim W 1999 *Japan. J. Appl. Phys.* **38** L174
[125] Hagelaar G J M, Kroesen G M W and Klein M H 2000 *J. Appl. Phys.* **88** 2240
[126] Yoon S and Lee I 2002 *J. Appl. Phys.* **91** 2487
[127] Piscitelli D, Pitchford L C and Boeuf J P 2000 *Int. Display Workshop* **IDW'00** 735
[128] Piscitelli D, Ganter R, Callegari T, Pitchford L C and Boeuf J P 2001 *Int. Display Workshop* **IDW'01** 825
[129] Piscitelli D, Revel I, Pitchford L C and Boeuf J P 2003 to be published
[130] Capdeville H, Pedoussat C and Pitchford L C 2001 *J. Appl. Phys.* **91** 1026
[131] Ziegler J F, Biersak J P and Littmark U 1985 *The Stopping and Range of Ions in Matter*

Downloaded from Plasma.com

[132] Mace C, Guillaumet S, Schwebel C and Aubert J 1999 *Proc. Eurodisplay 99* p 69
[133] Bechtel H, Jüstel T, Gläser H and Wiechert D U 2002 *J. SID* **10** 63
[134] Sahni O and Lanza C 1976 *J. Appl. Phys.* **47** 1337
[135] Veerasingam R, Campbell R B and McGrath R T 1995 *IEEE Trans. Plasma Sci.* **23** 688
[136] Veerasingam R, Campbell R B and McGrath R T 1996 *IEEE Trans. Plasma Sci.* **ED-24** 1399
[137] Takahashi K, Hashigushi S, Murakami Y, Takei M, Itoh K, Tachibana K and Sakai T 1996 *Japan. J. Appl. Phys.* **35** 251
[138] Veerasingam R, Campbell R B and McGrath R T 1997 *Plasma Sources Sci. Technol.* **6** 157
[139] McGrath R T, Veerasingam R, Hunter J A, Rockett P D and Campbell R B 1998 *IEEE Trans. Plasma Sci.* **26** 1532
[140] Uchiike H, Tuchiya N A H, Shinoda T and Fukushima Y 1984 *IEEE Trans. Electron Devices* **ED-31** 943
[141] Uchiike H, Fukuda M, Manabe A and Hirata T 1992 *SID*, *92* 543
[142] Boeuf J P and Doyeux H 1996 *Europhys. News* **27** 46
[143] Boeuf J P and Pitchford L C 1996 *IEEE Trans. Plasma Sci.* **24** 95
[144] Campbell R B, Veerasingam R and McGrath R T 1995 *IEEE Trans. Plasma Sci.* **ED-23** 698
[145] Veerasingam R, Campbell R B and McGrath R T 1996 *IEEE Trans. Plasma Sci.* **24** 1411
[146] Jeong H S, Shin B J and Whang K W 1999 *IEEE Trans. Plasma Sci.* **27** 171
[147] Rauf S and Kushner M J 1999 *J. Appl. Phys.* **85** 3470
[148] Veronis G and Inan U S 2002 *J. Appl. Phys.* **91** 9502
[149] Murakami Y, Matzuzaki H, Murakami K and Tachibana K 2000 *Japan. J. Appl. Phys.* **39** 590
[150] Drallos P J, Khudik V N and Nagorny V P 1998 *SID*, *98* 632
[151] Jeong H S, Murakami Y, Seki M and Murakami H 2001 *IEEE Trans. Plasma Sci.* **29** 559
[152] Kim H C, Hur M S, Yang S S, Shin S W and Lee J K 2002 *J. Appl. Phys.* **91** 9513
[153] Callegari T, Ouyang J, Lebarq N, Caillier B and Boeuf J P 2002 *International Display Research Conf., Eurodisplay 2002* p 735
[154] Ikeda Y, Suzuki K, Fukumoto H, Verboncoeur J P, Christenson P J, Birdsall C K, Shibata M and Ishigaki M 2000 *J. Appl. Phys.* **88** 6216
[155] Lee J K, Dagsteer S, Shon C H, Hur M S, Kim H C and Cho S 2001 *Japan. J. Appl. Phys.* **40** L528
[156] Hagelaar G J M, deHoog F J and Kroesen G M W 2000 *Phys. Rev.* E **62** 1452
[157] Hagelaar G L M and Kroesen G M W 2000 *J. Comp. Phys.* **159** 1
[158] Shon C H and Lee J K 2001 *Phys. Plasmas* **8** 1070
[159] Holstein T 1951 *Phys. Rev.* **83** 1159
[160] Hagelaar G J M, Klein M H, Snijkers R J M and Kroesen G M W 2000 *J. Appl. Phys.* **88** 5538
[161] Straaten T v d and Kushner M J 2000 *J. Appl. Phys.* **87** 2700
[162] Tamida T, Sanders S J and Tanaka M 2000 *Japan. J. Appl. Phys.* **39** 583
[163] Lee H J, Kim H C, Yang S S and Lee J K 2002 *Phys. Plasmas* **9** 2822
[164] Yoshioka T, Tessier L, Okigawa A and Toki K 2000 *J. SID* **8** 203
[165] Tachibana K, Kosugi N and Sakai T 1994 *Appl. Phys. Lett.* **65** 935
[166] Sawa M, Uchiike H, Zhang S and Yoshida K 1998 *SID*, *98*
[167] Sawa M, Uchiike H and Yoshida K 2000 *J. SID* **8** 163
[168] Yoon C K, Seo J H and Whang K W 2000 *IEEE Trans. Plasma Sci.* **28** 1029
[169] Jeong H S, Seo J H, Yoon C K, Kim J K and Whang K W 1999 *J. Appl. Phys.* **85** 3092
[170] Amemiya K, Nozu M, Torisaki Y, Uchidori M, Nishio T and Tamura M 1995 *Proc. Asia Display* **95** 965
[171] Callegari T, Ganter R and Boeuf J P 2000 *J. Appl. Phys.* **88** 3905
[172] Ganter R, Ouyang J, Callegari T and Boeuf J P 2002 *J. Appl. Phys.* **91** 992
[173] Ganter R, Ouyang J, Callegari T and Boeuf J P 2002 *J. Appl. Phys.* **91** 1000
[174] Kim J H, Lee J H, Whang K W and Choi Y W 2001 *J. Appl. Phys.* **89** 2539
[175] Noguchi Y, Matsuoka A, Bowden M D, Uchino K and Muraoka K 2001 *Japan. J. Appl. Phys.* **40** 326
[176] Noguchi Y, Matsuoka A, Uchino K and Muraoka K 2002 *J. Appl. Phys.* **91** 613
[177] Hagiwara K, Ushirozawa M, Jeong H S, Takano Y and Seki M 1998 *Int. Display Workshop* **IDW'98** 615
[178] Cho G, CHoi E H, Kim Y G, Kim D I, Uhm H S, Yoo Y D, Han J G, Kim M C and Kim J D 2000 *J. Appl. Phys.* **87** 4113
[179] Ganter R, Callegari T and Boeuf J P 2001 *J. SID* **9** 273
[180] Ouyang J, Ganter R, Callegari T and Boeuf J P 2002 *IEEE Trans. Plasma Sci.* **30** 186
[181] Vink T J, Verbeek R G F A and Zwart S T d 2000 *SID*, *00* 163
[182] Ouyang J, Callegari T, Lebarq N, Caillier B and Boeuf J P 2002 *International Display Research Conf., Eurodisplay 2002* p 53
[183] Oversluizen G, deZwart S, vanHeusden S and Dekker T 2000 *J. SID* **8** 197
[184] Oversluizen G, deZwart S, vanHeusden S and Dekker T 2001 *J. SID* **9** 267
[185] Yoshioka T, Miyakoshi A, Okigawa A, Mizobata E and Toki K 2000 *Int. Display Workshop* **IDW'00** 611
[186] Weber L F 2001 *US Patent* 6184848B1
[187] Kang J, Jeon W G, Kim O D, Song J W, Boeuf J P and Park M H 1999 *Int. Display Workshop* **IDW'99** 691
[188] Kang J, Kim O D, Jeon W G, Song J W, Park J, Lim J R and Boeuf J P 2000 *Int. Display Workshop* **IDW'00** 643
[189] Kurihara M and Makabe T 1999 *IEEE Trans. Plasma Sci.* **27** 1372
[190] Cany S, Kang J, Punset C and Boeuf J P 1999 *Int. Display Workshop* **IDW'99** 751
[191] Kang J 2000 *J. SID* **8** 223
[192] Surendra M 1995 *Plasma Sources Sci. Technol.* **4** 56
[193] Hargis P J *et al* 1994 *Rev. Sci. Instrum.* **65** 140
[194] Kanagu S, Kanazawa Y, Shinoda T, Yoshikawa K and Nanto T 1992 *SID*, *92* 713
[195] Seguin A, Tessier L, Doyeux H and Salavin S 1999 *Int. Display Workshop* **IDW'99** 699
[196] Bolsig *Bolzmann Equation Solver* http://www.siglo-kinema.com
[197] Piscitelli D, Phelps A V, Urquijo J d, Basurto E and Pitchford L C in preparation